of nestin-positive processes. Untransfected NPCs that were nestin positive had mainly long, bipolar processes (Fig. 3A, +bFGF). Cells that were transfected with a green fluorescent protein (GFP) expression vector (negative control) had a morphology that was similar to that of untransfected cells (Fig. 6A). By contrast, cells transfected with wild-type (WT) UCH-L1 cDNA had significantly shorter processes (47.6±6.4 μm, mean±s.e.m., n=81) than mock-transfected cells (69.9±7.0 μm, n=82) (Fig. 6A).

We then examined the relationship between the UCH-L1 structure and its activity with respect to morphological induction. We prepared two UCH-L1 mutants: D30A UCH-L1 lacked hydrolase activity and binding affinity for ubiquitin (Fig. 6B,C) (Osaka et al., 2003); C90S UCH-L1 lacked hydrolase activity but maintained binding affinity for ubiquitin (Fig. 6B,C) (Osaka et al., 2003). We compared the deubiquitylating activity of each UCH-L1 mutant using Ub-AMC as a substrate. The D30A mutant had little hydrolase activity, and the activity of the C90S mutant was not detectable (Fig. 6B; right). Sodium dodecyl sulfate-polyacrylamide gel electrophoresis revealed that there were no detectable contaminating proteins in these recombinant protein preparations (Fig. 6B; left). Co-immunoprecipitation experiments demonstrated that WT UCH-L1 and the C90S mutant physically associated with monoubiquitin. The D30A mutant (as well as GFP alone, which was used as a control) did not associate with ubiquitin (Fig. 6C). Although we did not detect a statistically significant difference, cells transfected with the D30A mutant tended to have longer nestin-positive processes (83.4±7.1 μm, n=87) as compared with cells transfected with the GFP expression vector (Fig. 6A). By contrast, cells transfected with the C90S mutant had significantly shorter fibers (39.3±4.5 μm, n=120; ANOVA: F=11.5, P<0.0001; Dunnett's multiple comparison test: GFP vs WT, P<0.05; GFP vs C90S, P<0.001; GFP vs D30A, P>0.05; Fig. 6A). We also compared the length of nestin-positive processes among UCH-L1 mutants (Bonferroni-Dunn Multiple Comparison Test: WT vs C90S, P=0.32; WT vs D30A, P<0.0001; D30A vs C90S, P<0.0001). Taken together, our data suggest that the effect of UCH-L1 expression on NPC morphology is dependent on the interaction between monoubiquitin and UCH-L1.

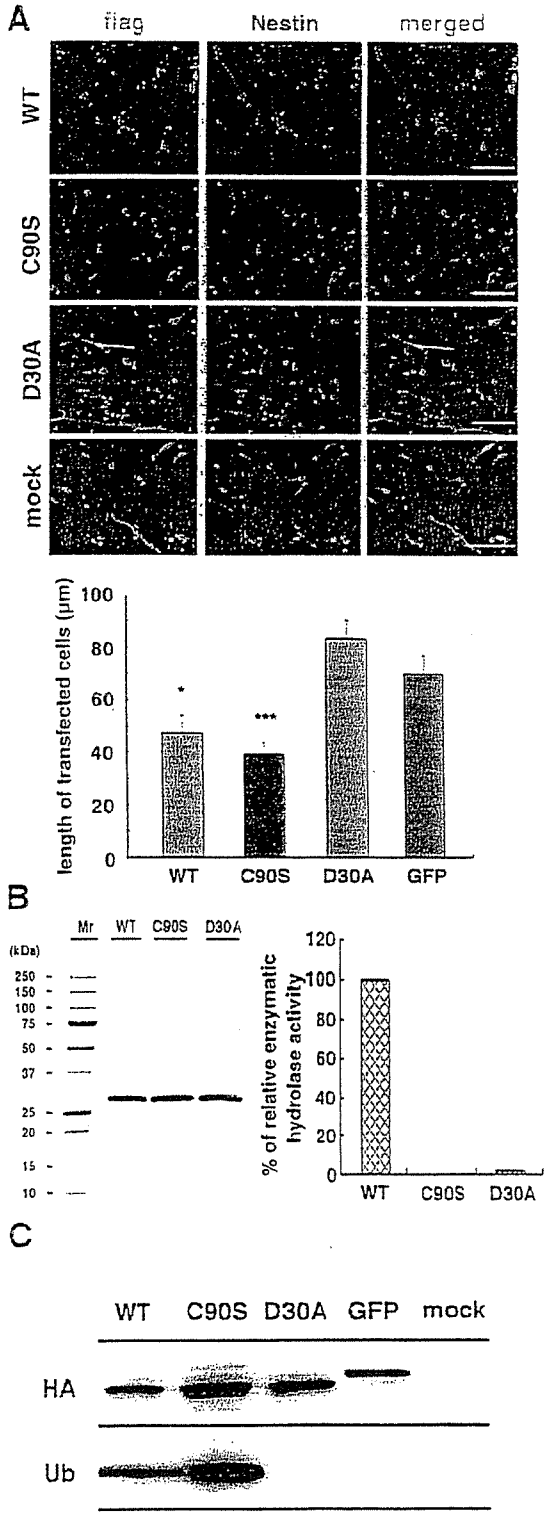

Fig. 6. The induction of short processes depends on the interaction between UCH-L1 and monoubiquitin. (A) FLAG-tagged WT UCH-L1, C90S UCH-L1, D30A UCH-L1 and GFP (all in the pCI-*neo* vector) were transfected into NPCs. Antibodies against the FLAG-tag were used to detect transfected UCH-L1. The green staining shows transfected cells and the red staining shows endogenous nestin. Transient transfection of each construct was performed under proliferating conditions. At 48 hours after transfection, bFGF was removed for 12 hours before the cultures were immunostained. The lengths of nestin-positive processes in immunostained cells were measured. Asterisks indicate differences from the value of GFP-transfected NPCs at $*P$<0.05 and $***P$<0.001. Bars, 80 μm. (B) Visualization of recombinant 6HN-tagged UCH-L1 by sodium dodecyl sulfate-polyacrylamide gel electrophoresis with Coomassie staining (B, left). UCH-L1 hydrolase activity was measured by Ub-AMC hydrolysis. Enzyme concentration was 4.3 nM, and substrate concentration was 700 nM. Initial velocity data was used to determine the values for relative hydrolase activity of UCH-L1 (B, right). (C) UCH-L1 co-immunoprecipitated with Ub. Cytosolic extracts from NIH-3T3 cell lines stably expressing HA-tagged WT UCH-L1 and mutants thereof were immunoprecipitated using anti-HA and immunoblotted with anti-HA antibody or anti-Ub antibody.

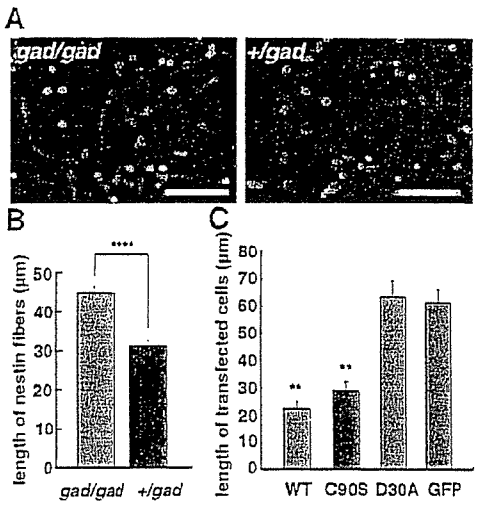

Fig. 7. A comparative experiment of *gad* mice and heterozygous littermates. The experiment compared *gad* mice (A,B) with a transfection study using FLAG-tagged WT UCH-L1, C90S UCH-L1, D30A UCH-L1 and GFP (mock) into *gad*-mouse-derived NPCs (C). The lengths of nestin-positive processes in immunostained cells were measured. NPCs from *gad* mice had longer nestin-positive processes compared with the control (A,B). (C) At 48 hours after transfection, bFGF was removed for 12 hours before the cultures were immunostained. The lengths of nestin-positive processes in immunostained cells were measured. Asterisks indicate differences from the value of GFP-transfected NPCs at $^{**}P<0.01$ and $^{****}P<0.0001$. Bar, 50 μm.

A comparative experiment using *gad*-mouse-derived NPCs

We did a comparative experiment using *gad* mice and heterozygous littermates. Nestin-positive NPCs from *gad* mice had longer processes. When we measured the length of nestin-positive fibers, NPCs from *gad* mice (45.0±1.4 μm, mean±s.e.m., n=366) had significantly longer nestin-positive processes compared with the control (31.4±1.3 μm, n=363) (Mann-Whitney U test: *gad* vs control, $P<0.0001$; Fig. 7A,B).

We next examined the effect of UCH-L1 on *gad*-mouse-derived NPCs using the transient transfection method. As observed in B6-derived cells, NPCs from *gad* mice that were transfected with WT UCH-L1 cDNA had significantly shorter processes (22.2±2.7 μm, mean±s.e.m., n=70) than mock-transfected cells (61.0±4.9 μm, n=88) (Bonferroni-Dunn multiple comparison test: GFP vs WT, $P<0.0001$) (Fig. 7C). Similarly, cells transfected with the C90S mutant had significantly shorter fibers (28.9±3.1 μm, n=71) (GFP vs C90S, $P<0.0001$). Although we did not detect a statistically significant difference, cells transfected with the D30A mutant tended to have longer nestin-positive processes (63.3±5.9 μm, n=80) as compared with cells transfected with the GFP expression vector (GFP vs D30A, P=0.70) (Fig. 7C). We also compared the length of nestin-positive processes among UCH-L1 mutants (Bonferroni-Dunn multiple comparison test: WT vs C90S, P=0.32; WT vs D30A, $P<0.0001$; D30A vs C90S, $P<0.0001$). Taken together, our data suggest that the effect of UCH-L1 expression on NPC morphology is dependent on the interaction between monoubiquitin and UCH-L1.

Discussion

UCH-L1 is a neuron-specific marker in the adult brain. In the present study, we provide experimental evidence that UCH-L1 is expressed in NPCs (Figs 2, 3). Using immunohistochemistry in the mouse brain, we detected UCH-L1 expression at E14 and E16. Interestingly, the expression pattern differed between E14 and E16 (Fig. 2). At E14, when the CP is forming, UCH-L1 expression was higher in the VZ than in the CP. At E14, the VZ contains progenitor cells that are generating neurons in the neocortex (Hashimoto and Mikoshiba, 2004; Malatesta et al., 2003). By contrast, UCH-L1 expression at E16 was lower in the VZ than in the CP. At E16, neuritogenesis and neuronal maturation are active in the CP, and gliogenesis is beginning in the VZ (Rice and Curran, 2001). The cerebral cortex layer becomes thicker at E16, where glial cells are not yet generated. The staining pattern for TuJ1 and nestin did not change between E14 and E16 (Fig. 2), indicating that UCH-L1 is highly expressed in the cortical layer prior to gliogenesis. The change in the expression pattern of UCH-L1 was coincident with the transition from neurogenesis to gliogenesis in the VZ. These results raise the possibility that UCH-L1 mediates not only the neuronal differentiation of NPCs but also the transition from neurogenesis to gliogenesis.

Time is a pivotal factor in the programmed sequence that produces neurons and glial cells from NPCs (Qian et al., 2000), in that the switch from neurogenesis to gliogenesis is regulated by time. The mechanism behind this progression of the progenitor cells is not well understood. Cultured NPCs generate neurons first, followed by astrocytes and then oligodendrocytes (Qian et al., 2000; Temple, 2001). This order of production for each population has been verified in vivo (Sauvageot and Stiles, 2002). The pattern of UCH-L1 immunoreactivity suggests that UCH-L1 is required for the onset of neurogenesis, which is followed by glial differentiation (Fig. 2).

We thus examined the role of UCH-L1 in neurogenesis using cultured NPCs. In UCH-L1/nestin double-staining experiments, the number of double-positive cells decreased with time in culture (Fig. 3). Conversely, UCH-L1 single-positive cells increased. In the double-staining experiments for UCH-L1 and TuJ1, the number of UCH-L1 single-positive cells decreased with time in culture, whereas the number of UCH-L1/TuJ1 double-positive cells increased (Fig. 4). These observations suggest that most UCH-L1-positive cells initially express nestin, but they express TuJ1 at a later stage. As we observed in vivo and in vitro (Figs 2-4), NPCs express UCH-L1, and its expression increases as the NPCs differentiate into neuronal cells. The number of nestin single-positive cells transiently increased before the UCH-L1 single-positive population increased (Fig. 3). The nestin single-positive population might have changed into the UCH-L1/nestin double-negative population (Fig. 3). Although the fate of the double-negative populations remains unknown, the double-negative cells might represent glial cells. Alternatively, some of the nestin single-positive cells might have changed into UCH-L1/nestin double-positive cells and then differentiated into UCH-L1 single-positive cells. A few UCH-L1-negative and TuJ1-positive cells were detected in the differentiating NPCs (Fig. 4). Thus, TuJ1-positive early neurons appear to be heterogeneous. UCH-L1/TuJ1 double-positive immunoreactivity suggested that UCH-L1 is not

absolutely required for some portion of neuronal cell development (Fig. 1B and Fig. 4A). This might explain why *gad* mouse neurons develop despite the absence of UCH-L1.

Because UCH-L1 was expressed in nestin-positive NPCs, we further examined the role of UCH-L1 in cell morphology (Fig. 5). Differentiating NPCs change morphology (Noctor et al., 2001), but the role of UCH-L1 in differentiating neurons has not been investigated. We classified nestin-positive cells based on the length of their processes. Nestin single-positive cells were predominantly long, whereas most UCH-L1/nestin double-positive cells were predominantly short (Fig. 5). These results suggest that UCH-L1 plays a role in regulating NPC process length. We examined this possibility by inducing UCH-L1 in nestin-positive cells. Untransfected, proliferating nestin-positive NPCs had mainly long and bipolar processes [Fig. 3A, bFGF (48 hours)], but when UCH-L1 was transfected, the length of nestin-positive NPC processes shortened (Fig. 6A). The unipolar population increased following UCH-L1 expression. These results support the idea that UCH-L1 regulates NPC morphology. This idea was further confirmed by observations in NPCs from *gad* mice; as shown in Fig. 7B, NPCs from homozygous *gad* mice had longer processes than those from heterozygous controls. In addition, we observed that transfection of UCH-L1 shortened the processes of NPCs from *gad* mice compared with mock transfectants (Fig. 7C).

Our results also suggest that at least two populations of NPCs exist in the embryonic brain. The populations can be classified by the presence or absence of UCH-L1. In the dentate gyrus of the adult mouse brain, there are two distinct subpopulations of nestin-positive cells (Fukuda et al., 2003): those having short processes differentiate into neurons, whereas those having long processes generate late progenitors, which have short processes. The nestin staining pattern of brains from *gad* mice differed from that of brains from heterozygous littermates (Fig. 1). In the *gad* mouse brain, nestin-positive radial fibers were prominent, and almost all progenitor cells appeared to have long processes (Fig. 1). Since UCH-L1 affected NPC morphology (Fig. 6A and Fig. 7C), the difference in vivo indicates that differentiation itself was modulated by the absence of UCH-L1. Considering that neurons are present in the *gad* mouse even though it lacks UCH-L1 expression, further investigation into the morphological role of UCH-L1 using various approaches including the BrdU studies should provide important information about the heterogeneity of cortical neurons.

UCHs hydrolyze ubiquitin C-terminal small adducts in vitro (Larsen et al., 1998). Recently, a significant relationship was reported between UCH-L1 hydrolase activity and cell proliferation in lung cancer cell lines (Liu et al., 2003). We previously demonstrated that UCH-L1 extends ubiquitin half-life and prevents ubiquitin degradation. This function depends on the interaction between UCH-L1 and monoubiquitin but not on hydrolase activity (Osaka et al., 2003). In the present study, WT UCH-L1 and the C90S mutant both decreased the length of NPC processes. Both molecules associate with monoubiquitin, unlike another mutant, D30A, which did not affect process length (Fig. 6). Similar results were obtained from the transfection study using nestin-positive NPCs from *gad* mice (Fig. 7C). Thus, the effect of UCH-L1 on NPC process length is dependent on the interaction between UCH-L1 and ubiquitin but not on hydrolase activity. Although we did not examine the ligase activity of each mutant (Liu et al., 2002), the C90S mutant is unlikely to have ligase activity, because conjugation of ubiquitin to the C90S mutant forms a stable complex that prevents the release of ubiquitin (Sullivan and Vierstra, 1993). This observation suggests that the ligase activity is not related to the morphological changes that occurred in NPCs.

The ubiquitin system has an essential role in various physiological events, including cell-cycle progression, specific gene transcription, membrane protein trafficking, reversal of stress damage and intracellular signaling (Weissman, 2001). In cortical neurogenesis, the role of the ubiquitin system is not well understood. Several molecules that are important in cortical neurogenesis, including Notch, P35 and Dabl, are ubiquitylated (Arnaud et al., 2003; Bock et al., 2004; Patrick et al., 1998; Qiu et al., 2000). Here we show for the first time that UCH-L1 is expressed in NPCs and regulates their morphology. In addition, in vivo UCH-L1 expression is localized to the VZ and cortical layers that are undergoing neurogenesis. Cells undergoing gliogenesis had little UCH-L1 expression in vivo. These results suggest that UCH-L1 facilitates neurogenesis, an activity that appears to depend on the affinity of UCH-L1 for ubiquitin.

Materials and Methods

Animals

Pregnant C57BL/6J mice were purchased from CLEA Japan. The *gad* mouse is an autosomal recessive mutant that was obtained by crossing CBA and RFM mice (Saigoh et al., 1999). The *gad* line was maintained by intercrossing for more than 20 generations (Kwon et al., 2003; Saigoh et al., 1999). All animal experiments were performed in the laboratory according to the NIH Standards for Treatment of Laboratory Animals.

Antibodies and reagents

Monoclonal and polyclonal antibodies used in this study were as follows: monoclonal anti-nestin antibody (Becton Dickinson; and Rat401, Developmental Studies Hybridoma Bank, The University of Iowa, Iowa City, IA), monoclonal anti-neuronal tubulin β III antibody (TuJ1; Covance), polyclonal anti-UCH-L1 antibody (PGP9.5; RA95101, UltraClone), and polyclonal anti-FLAG antibody (Sigma). All secondary polyclonal antibodies conjugated to Alexa Fluor fluorescein were purchased from Molecular Probes.

Cortical NPC culture and differentiation conditions in C57BL/6 mice

Cortical NPCs were cultured as previously described (Nakashima et al., 1999). Briefly, embryos were removed from pregnant C57BL/6J mice (CLEA Japan) and staged according to morphological criteria to confirm the gestational day (Kaufman et al., 1998). Developing mouse cerebral cortex was dissected from E14 embryos. Cells were mechanically dissociated by trituration and plated at a concentration of 3.0×10^6 cells per 10 cm dish (Becton Dickinson) precoated with 10 ml of 15 μg/ml poly-L-ornithine (Sigma) and 10 ml of 1 μg/ml fibronectin (Nitta Gelatin). Cells were expanded for 5 days in serum-free neurobasal (NB) medium (Invitrogen) supplemented with B27 (Invitrogen), 0.5 mM L-glutamine (Invitrogen), 100 U/ml penicillin and 100 μg/ml streptomycin (Invitrogen). This medium contained 10 ng/ml bFGF (PeproTech). Cultures were maintained at 37°C in an atmosphere of 95% air and 5% CO_2. For secondary culture, bFGF-expanded NPCs were washed in warm Hank's Balanced Salt Solution, detached with mechanical pipetting, and resuspended in NB medium supplemented with B27, but not bFGF. Cells were then replated in 24-well plates (Nunc; 1.8×10^5 cells per well) that were precoated with 500 μl of 15 μg/ml poly-L-ornithine and 500 μl of 1 μg/ml fibronectin for immunofluorescence staining at each time point.

Cortical NPC culture and differentiation conditions in *gad* mice

Culture of NPCs derived from *gad* mice was performed as with NPCs derived from B6 mice. Developing mouse cerebral cortex was dissected from embryos at E13.5 to E14.5. The precise gestational day was determined according to previously established morphological criteria (Kaufman et al., 1998). NPCs from each embryo were collected and cultured separately. Each genotype was determined later using PCR and, as a result, each pair of *gad* and control littermate mice from two sets of

parents were used. Each culture of NPCs was replated in 24-well plates without bFGF and stained using anti-UCH-L1 24 hours after plating.

Immunohistochemistry

Brain sections were stained as previously described (Li et al., 2003; Osaka et al., 2003). Briefly, E14 and E16 mouse brains were removed and fixed in 4% paraformaldehyde/phosphate-buffered saline (PBS) for 2 hours at room temperature, cryoprotected in 30% sucrose in PBS and frozen in dry ice. Sections (20 μm thick) were cut on a cryostat, and mounted on aminopropylsilane (APS)-coated glass slides. They were then washed three times in PBS for 5 minutes, and blocked for 1 hour at room temperature with 3% bovine serum albumin, 2% (v/v) normal goat serum, and 0.2% (v/v) Triton X-100 in PBS (pH 7.4). Sections were incubated with primary antibodies [anti-nestin antibody (Rat401) 1:10; or anti-UCH-L1 antibody (RA95101) 1:4000; or anti-TuJ1 antibody, 1:1000] overnight at 4°C or for 2 hours at room temperature. After rinsing in PBS, the sections were incubated for 2 hours with diluted fluorescein-conjugated secondary antibody (1:200). The images were obtained with a confocal laser scanning TCS SL microscope, and detailed analyses were performed using an LSC confocal microscope system (Leica). Immunofluorescence intensities were measured from confocal images with Mac SCOPE software (version 2.59; Mitani).

Immunocytochemistry

Cells were stained as previously described (Aoki et al., 2002). Briefly, all incubations and washes were performed at room temperature. Cells were fixed with 3.8% formaldehyde/PBS for 10 minutes and permeabilized with 0.02% (v/v) Triton X-100/PBS for 5 minutes. Fixed cells were blocked with 3.3% goat serum for 30 minutes. Cells were incubated with a diluted primary polyclonal or monoclonal antibody (both were used for double staining) for 0.5-1 hour. The cells were then incubated with diluted secondary antibody conjugated to fluorescein for 0.5-1 hour. Antibody dilutions were as follows: anti-UCH-L1 antibody, 1:4000; anti-nestin antibody, 1:500; anti-TuJ1, 1:500. All secondary antibodies were diluted 1:200 in 1% goat serum/PBS before use. The images were obtained with fluorescence microscopy on an IX70 microscope (Olympus).

Transfection

For C57BL/6 mice, cells replated in 24-well plates were cultured overnight in growth medium containing bFGF and B27. The next day, each construct was transfected using Lipofectamine 2000 (Invitrogen) according to the manufacturer's instructions. NPCs were allowed to proliferate for 48 hours after transfection and then induced to differentiate for 12 hours without bFGF. For *gad*-mouse-derived NPCs, transfection was done in a similar manner.

Expression plasmids for human UCH-L1 variants

Mutant cDNAs encoding human UCH-L1 containing either the D30A or C90S substitution were obtained using the QuikChange site-directed mutagenesis kit (Stratagene) with the following mutagenesis oligonucleotides: 5′-CAGTGGCGCTTCGTGGCCGTGCTGGGGCTGGAAG-3′ and 5′-CTTCCAGCCCCAGCACGGCCACGAAGCGCCACTG-3′ for D30A; 5′-CCATTGGGAATTCCTCTGGCACAATCGGAC-3′ and 5′-GTCCGATTGTGCCACAGGAATTCCCAATGG-3′ for C90S. Each single-nucleotide mutation in the resulting plasmids was confirmed by sequencing. Mammalian expression plasmids containing either FLAG-tagged human WT UCH-L1 or the D30A or C90S mutants were constructed using a pCI-*neo* mammalian expression vector (Promega). Bacterial expression plasmids containing either 6HN-tagged human WT UCH-L1 or the D30A or C90S mutants were constructed using a tetracycline-inducible expression system. *Xho*I-*Not*I cDNA fragments of the pCI-*neo* WT UCH-L1 or the D30A and C90S mutants and constructs were digested, and the DNA fragments were ligated between the *Sal*I and *Not*I sites in pPROtetE233 (Clontech) to generate pPROtetE233 6HN-tagged human WT, D30A and C90S UCH-L1 vectors. These expression plasmids were confirmed by sequencing.

In vitro assay for human UCH-L1 activity

Purified human UCH-L1 and the fluorogenic substrate ubiquitin-7-amino-4-methylcoumarin (Ub-AMC; Boston Biochem) were used to determine steady-state kinetic parameters as described previously (Nishikawa et al., 2003).

Immunoprecipitation

NIH-3T3 cells stably expressing human WT UCH-L1 or the C90S or D30A mutants, all with an HA-FLAG double tag at the N terminus, were cultured to subconfluency in a 10 cm dish, lyzed with 1 ml of modified RIPA buffer [50 mM Tris-HCl, pH 7.5, 1% (v/v) NP-40, 0.25% sodium deoxycholate, 150 mM NaCl, 1 mM EDTA] with EDTA-free complete protease inhibitor cocktail (Roche), sonicated and centrifuged at 18,000 *g* for 20 minutes at 4°C. Immunoprecipitation was performed as described previously (Ogawa et al., 2002).

Statistics

Statistical analyses were performed using StatView, version 5.0 (SAS) and Prism, version 3 (GraphPad Software). Analysis of variance (ANOVA) was used to assess differences between groups. A P value of less than 0.05 was considered statistically significant. When ANOVA results were statistically significant, they were examined by Fisher's PLSD, or Dunnett's multiple comparison test, or Bonferroni-Dunn multiple comparisons post hoc test. Differences between *gad* mice and control mice were analyzed using the Mann-Whitney U test.

The authors thank Yuh Nung Jan and Hua-Shun Li for providing the immunohistochemistry methods; Yoshihiro Nakatani and Hidesato Ogawa for providing the retroviral expression system and immunoprecipitation methods; and Masako Shikama for the care and breeding of animals. This work was supported by Grants-in-Aid for Scientific Research from the Ministry of Health, Labour and Welfare of Japan, and Grants-in-Aid for Scientific Research from the Ministry of Education, Culture, Sports, Science and Technology of Japan.

References

Aoki, S., Su, Q., Li, H., Nishikawa, K., Ayukawa, K., Hara, Y., Namikawa, K., Kiryu-Seo, S., Kiyama, H. and Wada, K. (2002). Identification of an axotomy-induced glycosylated protein, AIGP1, possibly involved in cell death triggered by endoplasmic reticulum-Golgi stress. *J. Neurosci.* 22, 10751-10760.

Arnaud, L., Ballif, B. A. and Cooper, J. A. (2003). Regulation of protein tyrosine kinase signaling by substrate degradation during brain development. *Mol. Cell. Biol.* 23, 9293-9302.

Bock, H. H., Jossin, Y., May, P., Bergner, O. and Herz, J. (2004). Apolipoprotein E receptors are required for reelin-induced proteasomal degradation of the neuronal adaptor protein Disabled-1. *J. Biol. Chem.* 279, 33471-33479.

Dickson, D. W., Schmidt, M. L., Lee, V. M., Zhao, M. L., Yen, S. H. and Trojanowski, J. Q. (1994). Immunoreactivity profile of hippocampal CA2/3 neurites in diffuse Lewy body disease. *Acta Neuropathol. (Berl.)* 87, 269-276.

Fukuda, S., Kato, F., Tozuka, Y., Yamaguchi, M., Miyamoto, Y. and Hisatsune, T. (2003). Two distinct subpopulations of nestin-positive cells in adult mouse dentate gyrus. *J. Neurosci.* 23, 9357-9366.

Hartfuss, E., Forster, E., Bock, H. H., Hack, M. A., Leprince, P., Luque, J. M., Herz, J., Frotscher, M. and Gotz, M. (2003). Reelin signaling directly affects radial glia morphology and biochemical maturation. *Development* 130, 4597-4609.

Hashimoto, M. and Mikoshiba, K. (2004). Neuronal birthdate-specific gene transfer with adenoviral vectors. *J. Neurosci.* 24, 286-296.

Kaufman, M. H., Brune, R. M., Davidson, D. R. and Baldock, R. A. (1998). Computer-generated three-dimensional reconstructions of serially sectioned mouse embryos. *J. Anat.* 193, 323-336.

Kawauchi, T., Chihama, K., Nabeshima, Y. and Hoshino, M. (2003). The in vivo roles of STEF/Tiam1, Rac1 and JNK in cortical neuronal migration. *EMBO J.* 22, 4190-4201.

Kwon, J., Kikuchi, T., Setsuie, R., Ishii, Y., Kyuwa, S. and Yoshikawa, Y. (2003). Characterization of the testis in congenitally ubiquitin carboxy-terminal hydrolase-1 (Uch-L1) defective (gad) mice. *Exp. Anim.* 52, 1-9.

Larsen, C. N., Krantz, B. A. and Wilkinson, K. D. (1998). Substrate specificity of deubiquitinating enzymes: ubiquitin C-terminal hydrolases. *Biochemistry* 37, 3358-3368.

Leroy, E., Boyer, R., Auburger, G., Leube, B., Ulm, G., Mezey, E., Harta, G., Brownstein, M. J., Jonnalagada, S., Chernova, T. et al. (1998). The ubiquitin pathway in Parkinson's disease. *Nature* 395, 451-452.

Li, H. S., Wang, D., Shen, Q., Schonemann, M. D., Gorski, J. A., Jones, K. R., Temple, S., Jan, L. Y. and Jan, Y. N. (2003). Inactivation of Numb and Numblike in embryonic dorsal forebrain impairs neurogenesis and disrupts cortical morphogenesis. *Neuron* 40, 1105-1118.

Liu, Y., Fallon, L., Lashuel, H. A., Liu, Z. and Lansbury, P. T., Jr (2002). The UCH-L1 gene encodes two opposing enzymatic activities that affect alpha-synuclein degradation and Parkinson's disease susceptibility. *Cell* 111, 209-218.

Liu, Y., Lashuel, H. A., Choi, S., Xing, X., Case, A., Ni, J., Yeh, L. A., Cuny, G. D., Stein, R. L. and Lansbury, P. T., Jr (2003). Discovery of inhibitors that elucidate the role of UCH-L1 activity in the H1299 lung cancer cell line. *Chem. Biol.* 10, 837-846.

Malatesta, P., Hartfuss, E. and Gotz, M. (2000). Isolation of radial glial cells by fluorescent-activated cell sorting reveals a neuronal lineage. *Development* 127, 5253-5263.

Malatesta, P., Hack, M. A., Hartfuss, E., Kettenmann, H., Klinkert, W., Kirchhoff, F. and Gotz, M. (2003). Neuronal or glial progeny: regional differences in radial glia fate. *Neuron* 37, 751-764.

McQuaid, S., McConnell, R., McMahon, J. and Herron, B. (1995). Microwave antigen retrieval for immunocytochemistry on formalin-fixed, paraffin-embedded post-mortem CNS tissue. *J. Pathol.* 176, 207-216.

Nadarajah, B., Brunstrom, J. E., Grutzendler, J., Wong, R. O. and Pearlman, A. L. (2001). Two modes of radial migration in early development of the cerebral cortex. *Nat. Neurosci.* 4, 143-150.

Nakashima, K., Yanagisawa, M., Arakawa, H., Kimura, N., Hisatsune, T., Kawabata, M., Miyazono, K. and Taga, T. (1999). Synergistic signaling in fetal brain by STAT3-Smad1 complex bridged by p300. *Science* 284, 479-482.

Nishikawa, K., Li, H., Kawamura, R., Osaka, H., Wang, Y. L., Hara, Y., Hirokawa, T., Manago, Y., Amano, T., Noda, M. et al. (2003). Alterations of structure and

hydrolase activity of parkinsonism-associated human ubiquitin carboxyl-terminal hydrolase L1 variants. *Biochem. Biophys. Res. Commun.* 304, 176-183.

Noctor, S. C., Flint, A. C., Weissman, T. A., Dammerman, R. S. and Kriegstein, A. R. (2001). Neurons derived from radial glial cells establish radial units in neocortex. *Nature* 409, 714-720.

Noctor, S. C., Flint, A. C., Weissman, T. A., Wong, W. S., Clinton, B. K. and Kriegstein, A. R. (2002). Dividing precursor cells of the embryonic cortical ventricular zone have morphological and molecular characteristics of radial glia. *J. Neurosci.* 22, 3161-3173.

Noctor, S. C., Martinez-Cerdeno, V., Ivic, L. and Kriegstein, A. R. (2004). Cortical neurons arise in symmetric and asymmetric division zones and migrate through specific phases. *Nat. Neurosci.* 7, 136-144.

Ogawa, H., Ishiguro, K., Gaubatz, S., Livingston, D. M. and Nakatani, Y. (2002). A complex with chromatin modifiers that occupies E2F- and Myc-responsive genes in G0 cells. *Science* 296, 1132-1136.

Osaka, H., Wang, Y. L., Takada, K., Takizawa, S., Setsuie, R., Li, H., Sato, Y., Nishikawa, K., Sun, Y. J., Sakurai, M. et al. (2003). Ubiquitin carboxy-terminal hydrolase L1 binds to and stabilizes monoubiquitin in neuron. *Hum. Mol. Genet.* 12, 1945-1958.

Patrick, G. N., Zhou, P., Kwon, Y. T., Howley, P. M. and Tsai, L. H. (1998). p35, the neuronal-specific activator of cyclin-dependent kinase 5 (Cdk5) is degraded by the ubiquitin-proteasome pathway. *J. Biol. Chem.* 273, 24057-24064.

Qian, X., Goderie, S. K., Shen, Q., Stern, J. H. and Temple, S. (1998). Intrinsic programs of patterned cell lineages in isolated vertebrate CNS ventricular zone cells. *Development* 125, 3143-3152.

Qian, X., Shen, Q., Goderie, S. K., He, W., Capela, A., Davis, A. A. and Temple, S. (2000). Timing of CNS cell generation: a programmed sequence of neuron and glial cell production from isolated murine cortical stem cells. *Neuron* 28, 69-80.

Qiu, L., Joazeiro, C., Fang, N., Wang, H. Y., Elly, C., Altman, Y., Fang, D., Hunter, T. and Liu, Y. C. (2000). Recognition and ubiquitination of Notch by Itch, a hect-type E3 ubiquitin ligase. *J. Biol. Chem.* 275, 35734-35737.

Rice, D. S. and Curran, T. (2001). Role of the reelin signaling pathway in central nervous system development. *Annu. Rev. Neurosci.* 24, 1005-1039.

Roegiers, F. and Jan, Y. N. (2004). Asymmetric cell division. *Curr. Opin. Cell Biol.* 16, 195-205.

Saigoh, K., Wang, Y. L., Suh, J. G., Yamanishi, T., Sakai, Y., Kiyosawa, H., Harada, T., Ichihara, N., Wakana, S., Kikuchi, T. et al. (1999). Intragenic deletion in the gene encoding ubiquitin carboxy-terminal hydrolase in gad mice. *Nat. Genet.* 23, 47-51.

Satoh, J. and Kuroda, Y. (2001). A polymorphic variation of serine to tyrosine at codon 18 in the ubiquitin C-terminal hydrolase-L1 gene is associated with a reduced risk of sporadic Parkinson's disease in a Japanese population. *J. Neurol. Sci.* 189, 113-117.

Sauvageot, C. M. and Stiles, C. D. (2002). Molecular mechanisms controlling cortical gliogenesis. *Curr. Opin. Neurobiol.* 12, 244-249.

Schofield, J. N., Day, I. N., Thompson, R. J. and Edwards, Y. H. (1995). PGP9.5, a ubiquitin C-terminal hydrolase; pattern of mRNA and protein expression during neural development in the mouse. *Brain Res. Dev. Brain Res.* 85, 229-238.

Sekiguchi, S., Yoshikawa, Y., Tanaka, S., Kwon, J., Ishii, Y., Kyuwa, S., Wada, K., Nakamura, S. and Takahashi, K. (2003). Immunohistochemical analysis of protein gene product 9.5, a ubiquitin carboxyl-terminal hydrolase, during placental and embryonic development in the mouse. *Exp. Anim.* 52, 365-369.

Shen, Q., Qian, X., Capela, A. and Temple, S. (1998). Stem cells in the embryonic cerebral cortex: their role in histogenesis and patterning. *J. Neurobiol.* 36, 162-174.

Sullivan, M. L. and Vierstra, R. D. (1993). Formation of a stable adduct between ubiquitin and the Arabidopsis ubiquitin-conjugating enzyme, AtUBC1+. *J. Biol. Chem.* 268, 8777-8780.

Tabata, H. and Nakajima, K. (2003). Multipolar migration: the third mode of radial neuronal migration in the developing cerebral cortex. *J. Neurosci.* 23, 9996-10001.

Temple, S. (2001). The development of neural stem cells. *Nature* 414, 112-117.

Weissman, A. M. (2001). Themes and variations on ubiquitylation. *Nat. Rev. Mol. Cell. Biol.* 2, 169-178.

Wilkinson, K. D., Lee, K. M., Deshpande, S., Duerksen-Hughes, P., Boss, J. M. and Pohl, J. (1989). The neuron-specific protein PGP 9.5 is a ubiquitin carboxyl-terminal hydrolase. *Science* 246, 670-673.

Zhong, W., Feder, J. N., Jiang, M. M., Jan, L. Y. and Jan, Y. N. (1996). Asymmetric localization of a mammalian numb homolog during mouse cortical neurogenesis. *Neuron* 17, 43-53.

Zhong, W., Jiang, M. M., Weinmaster, G., Jan, L. Y. and Jan, Y. N. (1997). Differential expression of mammalian Numb, Numblike and Notch1 suggests distinct roles during mouse cortical neurogenesis. *Development* 124, 1887-1897.

American Journal of Pathology, Vol. 169, No. 1, July 2006

DOI: 10.2353/ajpath.2006.060085

Cell Injury, Repair, Aging and Apoptosis

Photoreceptor Cell Apoptosis in the Retinal Degeneration of *Uchl3*-Deficient Mice

Yae Sano,*† Akiko Furuta,* Rieko Setsuie,*† Hisae Kikuchi,* Yu-Lai Wang,* Mikako Sakurai,*† Jungkee Kwon,*‡ Mami Noda,† and Keiji Wada*

From the Department of Degenerative Neurological Diseases, National Institute of Neuroscience, National Center of Neurology and Psychiatry, Tokyo, Japan; the Laboratory of Pathophysiology,† Graduate School of Pharmaceutical Sciences, Kyushu University, Fukuoka, Japan; and the Laboratory of Animal Medicine,‡ College of Veterinary Medicine, Chonbuk National University, Jeonju, Korea*

UCH-L3 belongs to the ubiquitin C-terminal hydrolase family that deubiquitinates ubiquitin-protein conjugates in the ubiquitin-proteasome system. A murine *Uchl3* deletion mutant displays retinal degeneration, muscular degeneration, and mild growth retardation. To elucidate the function of UCH-L3, we investigated histopathological changes and expression of apoptosis- and oxidative stress-related proteins during retinal degeneration. In the normal retina, UCH-L3 was enriched in the photoreceptor inner segment that contains abundant mitochondria. Although the retina of *Uchl3*-deficient mice showed no significant morphological abnormalities during retinal development, prominent retinal degeneration became manifested after 3 weeks of age associated with photoreceptor cell apoptosis. Ultrastructurally, a decreased area of mitochondrial cristae and vacuolar changes were observed in the degenerated inner segment. Increased immunoreactivities for manganese superoxide dismutase, cytochrome *c* oxidase I, and apoptosis-inducing factor in the inner segment indicated mitochondrial oxidative stress. Expression of cytochrome c, caspase-1, and cleaved caspase-3 did not differ between wild-type and mutant mice; however, immunoreactivity for endonuclease G was found in the photoreceptor nuclei in the mutant retina. Hence, loss of UCH-L3 leads to mitochondrial oxidative stress-related photoreceptor cell apoptosis in a caspase-independent manner. Thus, *Uchl3*-deficient mice represent a model for adult-onset retinal degeneration associated with mitochondrial impairment. *(Am J Pathol 2006, 169:132–141; DOI: 10.2353/ajpath.2006.060085)*

The ubiquitin system has been implicated in numerous cellular processes, including protein quality control, cell cycle, cell proliferation, signal transduction, membrane protein internalization, and apoptosis.[1,2] Ubiquitin-dependent processes are regulated by ubiquitinating enzymes, E1, E2, and E3, and deubiquitinating enzymes such as ubiquitin-specific proteases and ubiquitin C-terminal hydrolases (UCHs).[1,3–5] To date, four isozymes of UCHs, UCH-L1, UCH-L3, UCH-L4, and UCH-L5, have been cloned in mouse or human.[6–8] UCH-L1, also known as PGP 9.5, has been well characterized among the isozymes. UCH-L1 is selectively localized to brains and testis/ovaries[7] and functions as a ubiquitin ligase in addition to a deubiquitinating enzyme.[9] Furthermore, two distinct mutations are linked to Parkinson's disease in human[10] and gracile axonal dystrophy (*gad*) in mice.[11] UCH-L3, on the other hand, displays 52% amino acid identity to UCH-L1.[12] Uchl3 mRNA is expressed throughout various tissues and is especially enriched in testis and thymus.[13] In addition to its ubiquitin hydrolase activity, *in vitro* studies indicate that UCH-L3 cleaves the C terminus of the ubiquitin-like protein Nedd-8.[14,15] Although UCH-L1 and UCH-L3 are suggested to function as reciprocal modulators of germ cell apoptosis in experimental cryptorchid testis,[16] the cellular localization and function of UCH-L3 remain unknown in other organs.

Recently, *Uchl3*-deficient mice were generated with a deletion of exons 3 to 7, which are essential for hydrolase

Supported by grants-in-aid for scientific research from the Japan Society for the Promotion of Science; for priority area research from the Ministry of Education, Culture, Sports, Science and Technology, Japan; Kyushu University Foundation for Scientific Research from the Ministry of Health, Labour and Welfare, Japan; and the program for Promotion of Fundamental Studies in Health Sciences from the National Institute of Biomedical Innovation, Japan.

Accepted for publication March 23, 2006.

Address reprint requests to Akiko Furuta, M.D., Ph.D., Department of Degenerative Neurological Diseases, National Institute of Neuroscience, National Center of Neurology and Psychiatry, 4-1-1, Ogawahigashi, Kodaira, Tokyo 187-8502, Japan. E-mail: afuruta@ncnp.go.jp.

activity.[13] These mutant mice display postnatal retinal and muscular degenerations as well as mild growth retardation.[17] Retinal development is morphologically normal, but progressive retinal degeneration is reported to be evident at 3 months after birth.[17] However, precise chronological changes and the mechanism of the retinal degeneration in *Uchl3*-deficient mice has not been studied.

Both the caspase-dependent pathway and the caspase-independent pathway have been proposed to be involved in the models of retinal degeneration, including model animals for retinitis pigmentosa (such as Royal College of Surgeons (RCS) rat and retinal degeneration (*rd*) mice),[18] retinal detachment,[19] light injury,[20,21] ischemic injury,[22] and age-related macular degeneration.[23] In the ubiquitin system, UCH-L1 is involved in ischemia-induced apoptosis in the inner retina.[24] The role of UCH-L3 in retinal degeneration, however, is unclear.

To elucidate the function of UCH-L3, we investigated the histopathological changes and protein expression with respect to apoptotic pathways in *Uchl3*-deficient mice. Our results show that UCH-L3 is mainly localized to the photoreceptor inner segment that contains abundant mitochondria in the normal retina. *Uchl3*-deficient mice displayed caspase-independent apoptosis during postnatal retinal degeneration associated with increased expression of the markers for mitochondrial oxidative stress at the inner segment. We propose a possible antiapoptotic role of UCH-L3 in photoreceptor cells.

Materials and Methods

Animals

We used age-matched *Uchl3*-deficient mice and wild-type mice, all of which were offspring male from 15 to 20 pairs of heterozygotes that had been backcrossed with C57BL/6J at postnatal ages of 0 days (P0), 10 days (P10), 3 weeks (3w), 6 weeks (6w), 8 weeks (8w), and 12 weeks (12w). The total number of wild-type and *Uchl3*-deficient mice examined in the present study was 79, of which 30 mice were used for Western blotting, 42 mice were used for hematoxylin and eosin staining, immunohistochemistry, and terminal deoxynucleotidyl transferase-mediated dUTP nick end labeling (TUNEL) assay, and 7 mice were used for electron microscopy. The mice were maintained at the National Institute of Neuroscience, National Center of Neurology and Psychiatry (Tokyo, Japan). The experiments using the mice were approved by the Institute's Animal Investigation Committee.

Western Blotting

Eyes from P10-, 3w-, and 6w-old mice of both genotypes (10 mice in each time point, for a total of 30 mice) were lysed in protein lysis buffer (100 mmol/L Tris-HCl, pH 8.0, 300 mmol/L NaCl, 2% Triton X-100, 0.2% SDS, 2% sodium deoxycholate, 2 mmol/L EDTA) containing protease inhibitor (Complete protease inhibitor cocktail; Sigma-Aldrich, St. Louis, MO). The amount of total protein of each sample was determined by the Bio-Rad protein assay (Bio-Rad, Hercules, CA) using bovine serum albumin as a standard. Total protein (50 μg/lane) was separated by 15% SDS-polyacrylamide gels (Perfect NT Gel, DRC, Tokyo, Japan). Proteins were transferred to immuno-Blot polyvinylidene difluoride membranes (Bio-Rad) and incubated with 5% skim milk in TBST (50 mmol/L Tris-HCl-buffered saline, pH 7.0, containing 0.05% Triton X-100) for 1 hour at room temperature. The membranes were incubated with a 1:1000 dilution of each primary antibody for UCH-L1, UCH-L3,[25] and β-actin (1:1000; Sigma-Aldrich) overnight at 4°C. For the preparation of anti-mouse UCH-L1 antibody, histidine-tagged mouse UCH-L1 (6His-mUCH-L1) was prepared as described previously[26] and used to generate a polyclonal antiserum in rabbit (Takara, Tokushima, Japan). The polyclonal antibody was purified by affinity chromatography. The specificity of this antibody to the mouse UCH-L1 was verified by Western blotting using brain lysates from *gad* mice and wild-type mice (data not shown). The membranes were washed in TBST and further incubated with antimouse or rabbit IgG-horseradish peroxidase conjugate (1:1000; Chemicon, Temecula, CA). After washing in TBST, the membranes were developed with the Super Signal West Dura or Femto Extended Duration Substrate (Pierce, Rockford, IL) and analyzed with a Chemilmager (Alpha Innotech, San Leandro, CA). Western blotting was performed five times per each antibody.

Morphometric Analysis and Immunohistochemistry of Retina

Mice of both genotypes at P0, P10, 3w, 6w, 8w, and 12w of age (7 mice in each time point, total of 42 mice) were deeply anesthetized with diethylether, decapitated, and the eyes removed, immersion-fixed with 4% paraformaldehyde overnight at 4°C, and embedded in paraffin wax. Deparaffinized sections were stained with hematoxylin and eosin and examined under an Axioplan2 microscope (Carl Zeiss, Oberkochen, Germany) at a magnification ×400, and the thickness of each layer was measured using WinRoof software (Mitani Shoji, Tokyo, Japan).

For immunohistochemical studies, 5-μm-thick sagittal sections at the level of the optic nerve were deparaffinized and treated with 1% hydrogen peroxide (H_2O_2) for 30 minutes, incubated with 1% skim milk in phosphate-buffered saline (PBS, pH 7.4) for 1 hour at room temperature followed by incubation overnight at 4°C with each primary antibody for UCH-L1 and UCH-L3[25] diluted 1:500 in 1% skim milk in PBS. To characterize apoptosis- and oxidative stress-related proteins, antibodies to the following proteins were used; apoptosis-inducing factor (AIF; 1:500, Chemicon), caspase-1 (1:100; Cell Signaling Technology, Beverly, MA), caspase-3 (1:1000; Cell Signaling Technology), cleaved caspase-3 (1:50; Cell Signaling Technology), cytochrome *c* (1:1000; Santa Cruz Biotechnology, Santa Cruz, CA), cytochrome *c* oxidase I

(COX, 1:10,000; Molecular Probes, Eugene, OR), endonuclease G (Endo G; 1:500, Chemicon) and manganese superoxide dismutase (Mn-SOD; 1:10,000, Stressgen, Victoria, BC, Canada). The sections were washed in PBS and then incubated with biotinylated secondary antibodies diluted 1:500 in PBS containing 1% skim milk. The sections were treated with the VECTASTAIN Elite ABC kit (Vector Laboratories, Burlingame, CA) according to the manufacturer's protocol and developed with 0.02% 3,3′-diaminobenzidine tetrahydrochloride solution containing 0.003% H_2O_2. After visualization, sections were counterstained with hematoxylin. Sections were examined with an Axioplan2 microscope (Carl Zeiss). Immunohistochemistry was performed in at least three repeated experiments. The relative immunoreactivity for COX, Mn-SOD, AIF, and Endo G in each layer of mutant mice was compared with that of wild-type mice and was classified into no change (−), slight increase (±), mild increase (+), and marked increase (++).

TUNEL Staining

Apoptotic cells were examined in mice of both genotypes at P0, P10, 3w, 6w, 8w, and 12w (7 mice in each time point, for a total of 42 mice) by TUNEL stain using the Dead-End Fluorimetric TUNEL system kit (Promega, Madison, WI) according to the manufacturer's instructions. The sections were examined by using a confocal laser scanning microscope (Olympus, Tokyo, Japan). The microphotographs were captured at magnification ×400 (0.066 mm^2/each retinal section), positive cells were counted (Fluoview 2.0; Olympus), and the data were subjected to statistical analysis.

Electron Microscopic Analysis

3w-old mice of both genotypes (total 7 mice) were deeply anesthetized with 20% chloral hydrate aqueous solution and perfused with the following fixative: 2% paraformaldehyde, 2% glutaraldehyde in PBS, or sodium cacodylate buffer (pH 7.4). The eyes were removed and postfixed with the same fixative overnight at 4°C. The posterior segments of eyes were trimmed and washed with PBS or sodium cacodylate buffer, incubated in phosphate-buffered 1% osmium tetroxide for 1 hour, and dehydrated in ethanol and embedded in Epon 812 resin (TAAB, Berks, UK). Ultrathin sections (75 nm) were mounted on copper grids and stained with uranium acetate and lead citrate. The sections were observed using an H-7000 electron microscope (Hitachi, Tokyo, Japan). Morphometric analysis of mitochondria was performed by measuring average percentage of area occupied by cristae within a mitochondrion at the inner segment.

Statistical Analysis

In statistical analysis of thickness of retinal layers and TUNEL-positive cells, three wild-type and four *Uchl3*-deficient mice were used in each time point (P0, P10, 3w,

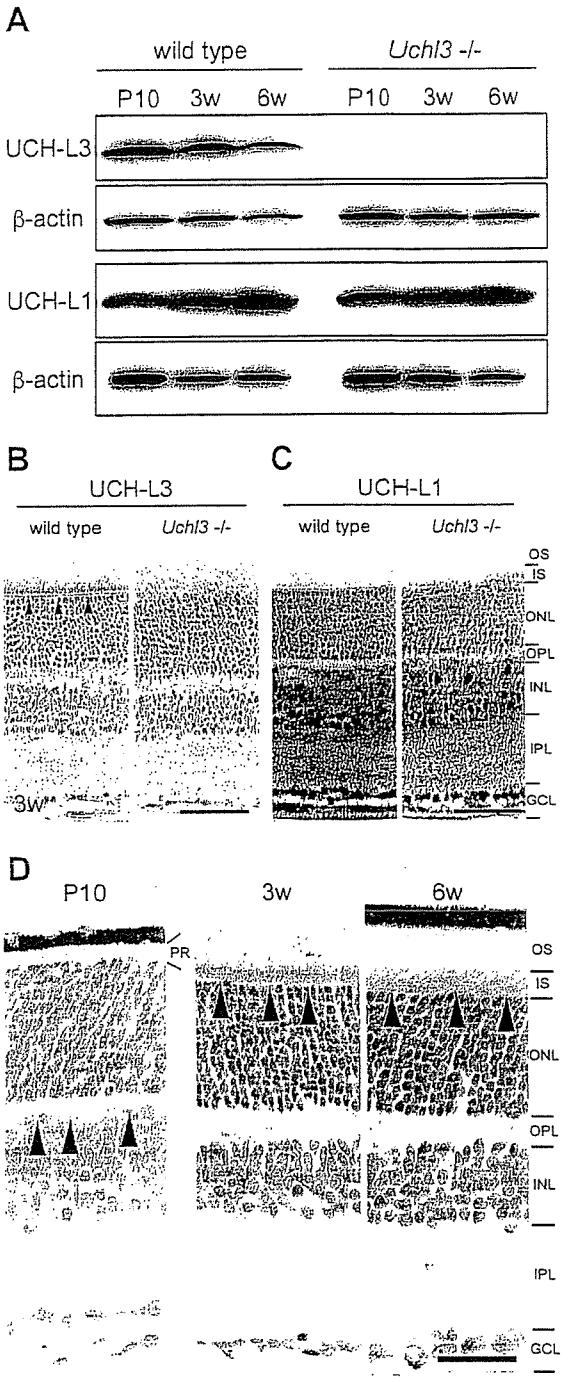

Figure 1. Expression of UCH-L1 and UCH-L3 in the retina of wild-type and *Uchl3*-deficient mice. **A:** Western blot analysis of UCH-L3 and UCH-L1 using whole-eye lysates from wild-type and *Uchl3*-deficient mice at P10, 3w, and 6w. The immunoreactive band for UCH-L3 is undetectable in *Uchl3*-deficient mice. Expression of UCH-L1 is similar between both genotypes. **B** and **C:** Immunohistochemistry for UCH-L3 (**B**) and UCH-L1 (**C**) in wild-type and *Uchl3*-deficient mice retinae at 3w. Immunoreactivity of UCH-L3 is found at the inner segment of the wild-type retina (**arrowheads**), whereas there is no significant immunoreactivity in *Uchl3*-deficient mice (**B**). UCH-L1 is expressed at the inner retina in both genotypes. **D:** Immunohistochemistry of UCH-L3 at P10, 3w, and 6w in wild-type retinae. UCH-L3 is faintly expressed in the outer plexiform layer at P10 (**arrowheads**). Thereafter, immunoreactivity for UCH-L3 is found in inner segment at 3w and 6w (**arrowheads**). PR, photoreceptor; OS, outer segment; IS, inner segment; ONL, outer nuclear layer; OPL, outer plexiform layer; INL, inner nuclear layer; IPL, inner plexiform layer; GCL, ganglion cell layer. Scale bars = 50 μm (**B** and **C**) and 20 μm (**D**).

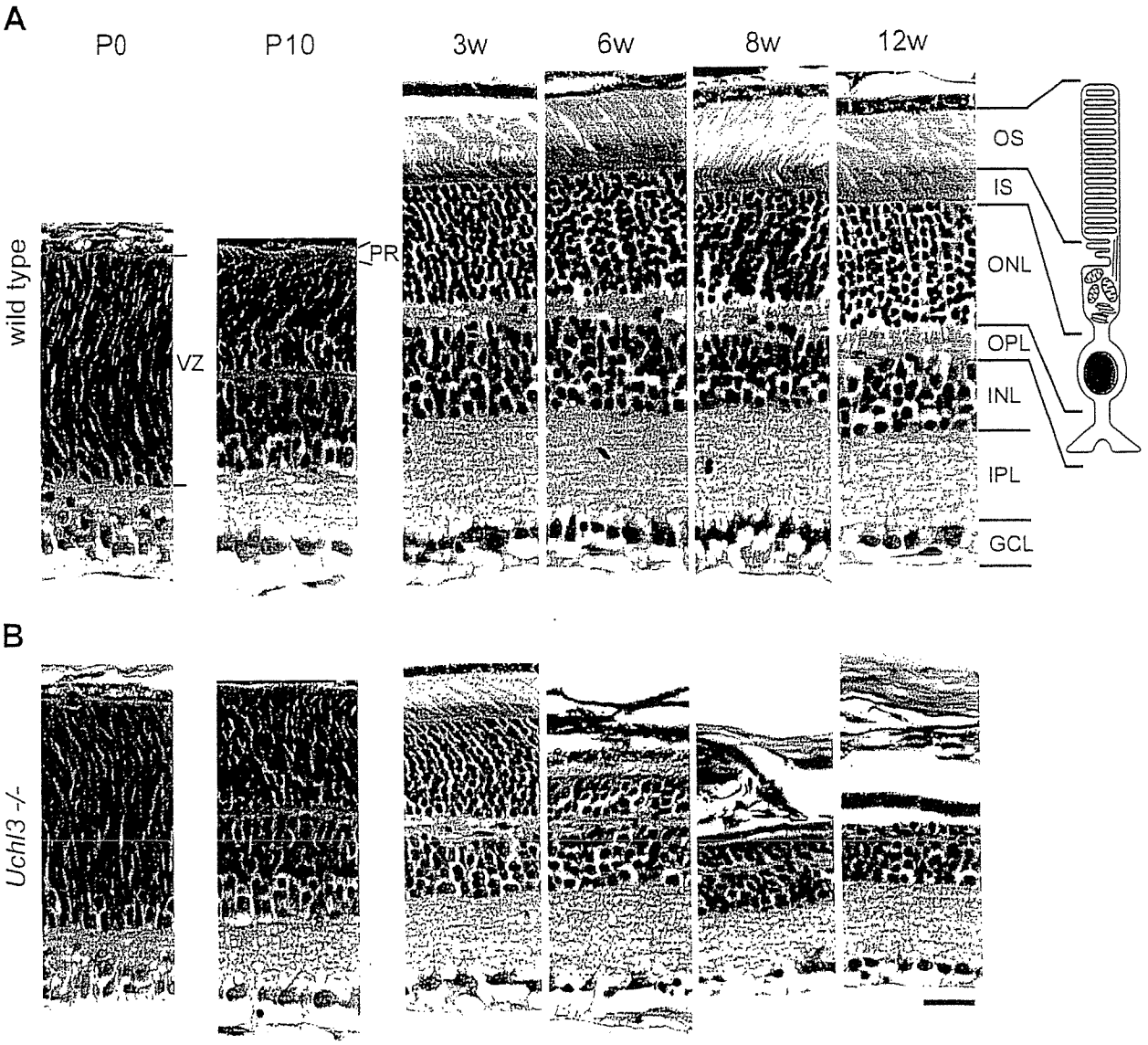

Figure 2. Histopathological changes of postnatal development in wild-type (**A**) and retinal degeneration of *Uchl3*-deficient mice (**B**) at P0, P10, 3w, 6w, 8w, and 12w. There is no morphological difference between both genotypes at P0 and P10, whereas outer and inner segments, outer nuclear layers, and outer plexiform layers are progressively degenerated after 3w of age. The illustration indicates a rod photoreceptor cell. VZ, ventricular zone; PR, photoreceptor; OS, outer segment; IS, inner segment; ONL, outer nuclear layer; OPL, outer plexiform layer; INL, inner nuclear layer; IPL, inner plexiform layer; GCL, ganglion cell layer. H&E staining. Scale bar = 20 μm (**A** and **B**).

6w, 8w, and 12w; for a total of 42 mice). The percentage of cristae area to whole mitochondrion in ultramicrophotographs was measured in 50 mitochondria of each genotype from three wild-type mice and four *Uchl3*-deficient mice, and the data were subjected to statistical analysis. All statistical analyses were carried out by Student's *t*-test using Microsoft Excel.

Results

Expression of UCH-L3 in the Murine Retina

Western blotting detected UCH-L3 (~30 kd) in extracts of eyes from wild-type mice at P10, 3w, and 6w, but the band was undetectable in *Uchl3*-deficient mice (Figure 1A). The expression level of UCH-L1 was similar in both genotypes. There was a tendency that the level of UCH-L3 decreased with age while the level of UCH-L1 increased with age in wild-type mice of all samples examined (five blots per antibody). Immunohistochemically, the cellular distribution of UCH-L3 differed from that of UCH-L1. UCH-L3 was enriched in the photoreceptor inner segment in wild-type mice at 3w of age (Figure 1B), whereas UCH-L1 was expressed in both genotypes in the inner retina, which consists of the inner nuclear layer, inner plexiform layer, and ganglion cell layer (Figure 1C). Localization of UCH-L3 in the wild-type retina was altered with age (Figure 1D). Immunoreactivity for UCH-L3 was not found at P0. UCH-L3 was faintly expressed in the outer plexiform layer at P10. Thereafter, it was localized to

inner segment at 3w. The inner segment was less immunoreactive for UCH-L3 at 6w, 8w, and 12w, compared with 3w.

Histopathological Changes of Retinal Degeneration in the Uchl3-Deficient Mice

Microscopic examination of retinal cross-sections revealed no obvious histopathological changes during early postnatal development at P0 and P10 in the retina of *Uchl3*-deficient mice (Figure 2). At 3w of age, the mutant retina began to degenerate in the inner segment and ultimately disappeared at 12w (Figures 2B and 3D). Thickness of the outer segment, outer nuclear layer, and outer plexiform layer was also significantly decreased in the mutant mice at 6w of age (Figure 3, C, E, and F). Despite the conspicuous change in the photoreceptor cells, the thickness of the mutant inner retina up to 12w of age was not altered compared with that of the wild-type (Figure 3, G–I).

Ultrastructurally, vacuolar changes were found in the inner segment of *Uchl3*-deficient mice at 3w of age (Figure 4). Mitochondria at the inner segment of mutant mice were slightly swollen. Groups of small round-to-oval structures were observed in the degenerated inner segment (Figure 4D), and these structures were considered to be the cross-sections of cell processes. Chromatin condensation in photoreceptor nuclei was sometimes seen in the outer nuclear layer at 3w (Figure 4F). Morphometric analysis showed that the percentage of cristae area to whole area of mitochondrion in the inner segment of *Uchl3*-deficient mice was significantly lower than that of wild-type mice (Figure 4, G and H).

Altered Expressions of Apoptosis-Related Proteins in the Degenerated Retina

Apoptotic cells in the retinal cross-sections were identified using the TUNEL staining. TUNEL-positive cells were identified in the ventricular zone at P0 and inner nuclear layer at P10 of both genotypes during the developmental period (Figure 5, A and C). The number of TUNEL-positive cells slightly increased in the inner nuclear layer at P10. After 3w of age, TUNEL-positive cells of mutant retina significantly increased at the outer nuclear layer of the mutant retina at 3w, 6w, and 8w (Figure 5, A and D).

To determine which apoptotic pathway was activated in *Uchl3*-deficient mice, we examined immunoreactivities of apoptosis-related proteins. Expression of cytochrome *c*, caspase-3, and cleaved caspase-3 and caspase-1, essential molecules for the caspase-dependent pathway, were unchanged in both genotypes (Figure 6A), whereas oxidative stress markers, COX and Mn-SOD as well as AIF and Endo G, indicators of the caspase-independent pathway, were altered in the mutant retina (Figure 6B). Chronological changes in expression of markers for oxidative stress and caspase-independent apoptosis at P0, P10, 3w, 6w, 8w, and 12w are shown in Table 1. The immunoreactivity of COX was increased in the inner segment at 3w and 6w. Mn-SOD was mildly increased in the inner segment at 3w, 6w, and 8w. Although AIF was enriched in the inner segment of *Uchl3*-deficient mice at 3w and 6w, nuclear labeling of AIF was not observed. On the other hand, Endo G was localized to the nuclei of the outer nuclear layer of the mutant retina at 3w and 6w. Expression of Endo G was slightly increased in the outer plexiform layer, inner nuclear layer, and inner plexiform layer of *Uchl3*-deficient mice after 3w of age (Table 1). Thus, degeneration of photoreceptor cells in *Uchl3*-defi-

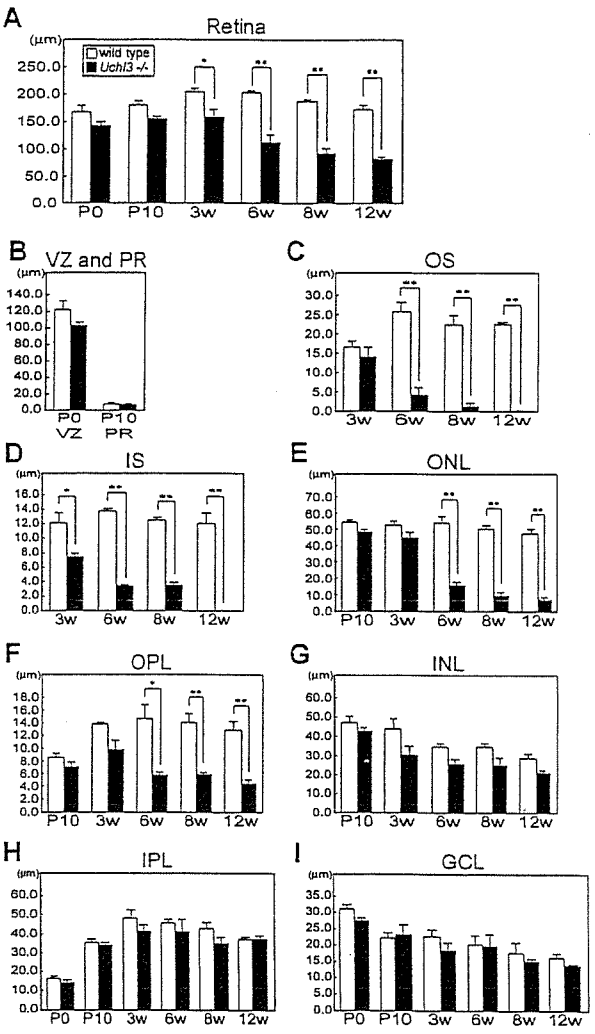

Figure 3. Chronological changes of retinal degeneration as assessed by thickness of each layer at different ages in wild-type and *Ucbl3*-deficient mice. **A:** Total retinal thickness is progressively decreased after 3w of age. **B:** Thickness of ventricular zone at P0 and photoreceptor layer at P10 shows no significant changes between both genotypes. **C–F:** Thickness of outer retinal layers in wild-type and *Ucbl3*-deficient mice at different ages. The earliest change is revealed at 3w of age in inner segment of mutant retina (**D**). Thickness of outer segment (**C**), outer nuclear layer (**E**), and outer plexiform layer (**F**) in *Ucbl3*-deficient mice is significantly decreased with age compared with that in the wild-type. **G–I:** Thickness of inner retinal layers in wild-type and *Ucbl3*-deficient mice at different ages. Thickness of inner nuclear layer (**G**), inner plexiform layer (**H**), and ganglion cell layer (**I**) are unchanged between both genotypes. Each value represents the mean ± SE ($^{*}P < 0.05$; $^{**}P < 0.01$). In all panels, the white bars represent the thickness in wild-type mice and the black bars represent the thickness in *Ucbl3*-deficient mice. VZ, ventricular zone; PR, photoreceptor; OS, outer segment; IS, inner segment; ONL, outer nuclear layer; OPL, outer plexiform layer; INL, inner nuclear layer; IPL, inner plexiform layer; GCL, ganglion cell layer.

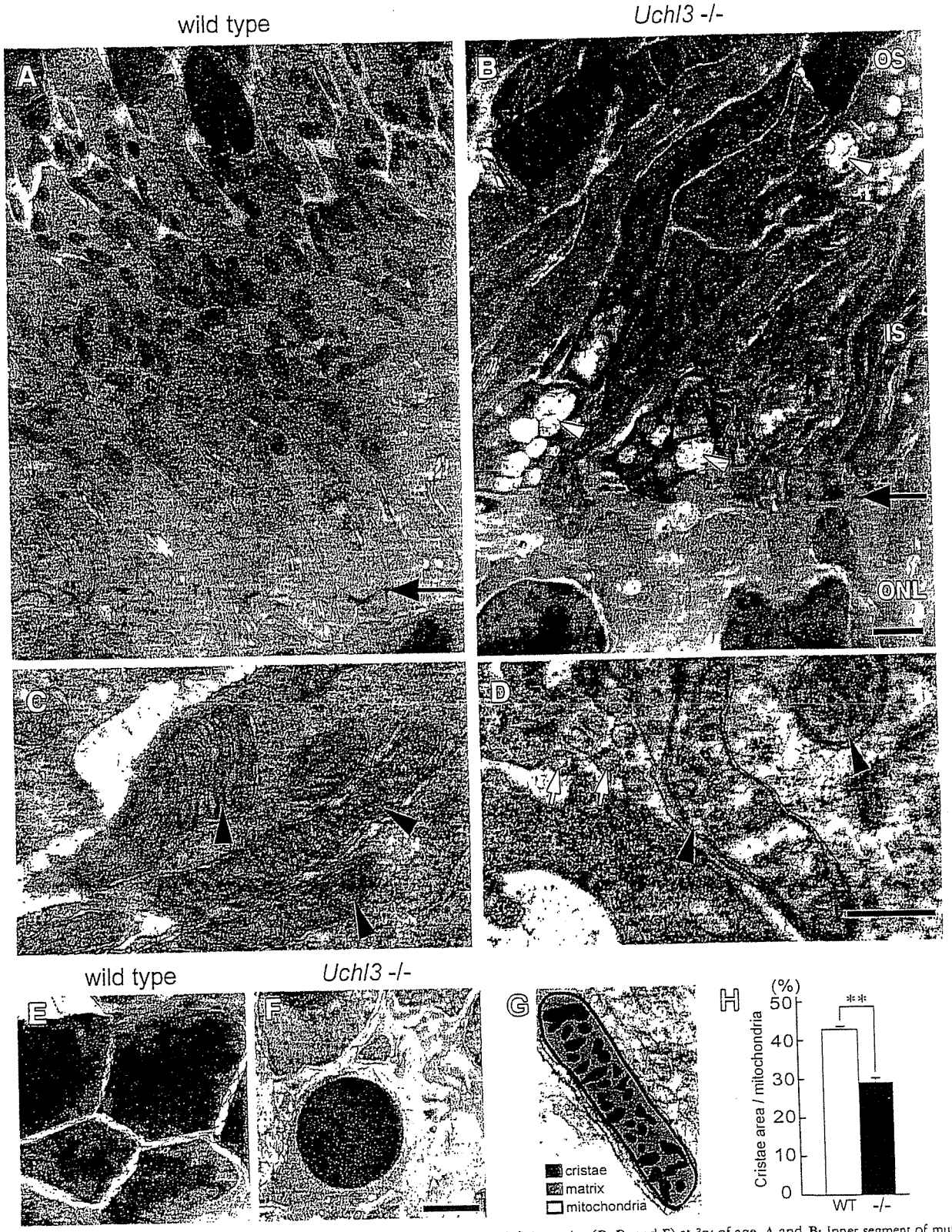

Figure 4. Ultrastructure of the outer retina in wild-type (**A**, **C**, and **E**) and *Uchl3*-deficient mice (**B**, **D**, and **F**) at 3w of age. **A** and **B:** Inner segment of mutant retina is shrunken associated with vacuolar changes (**arrowheads** in **B**). **Arrows** in **A** and **B** indicate outer limiting membrane. **C** and **D:** Subsets of mitochondria at the inner segment in *Uchl3*-deficient mice are swollen with decreased cristae (**arrowheads** in **D**) compared with that of wild-type (**arrowheads** in **C**). Groups of small round-to-oval shaped structures are occasionally seen in degenerated inner segment (**white arrows** in **D**). **E** and **F:** Outer nuclear layer of wild-type (**E**) and *Uchl3*-deficient (**F**) mice. Chromatin condensation of photoreceptor cells is observed in mutant mice (**F**). **G** and **H:** Morphometric analysis of mitochondria was performed with the percentage of cristae area (**G**; **red**) against mitochondrial area ($n = 50$ for each genotype). Cristae area in the inner segment is significantly decreased in mutant retina (**H**, $-/-$, **black bar**) compared with that in wild-type (**H**, WT, **white bar**). Each value represents the mean ± SE (**$P < 0.01$). OS, outer segment; IS, inner segment; ONL, outer nuclear layer. Scale bars = 1 μm (**A** and **B**), 500 nm (**C** and **D**), and 1 μm (**E** and **F**).

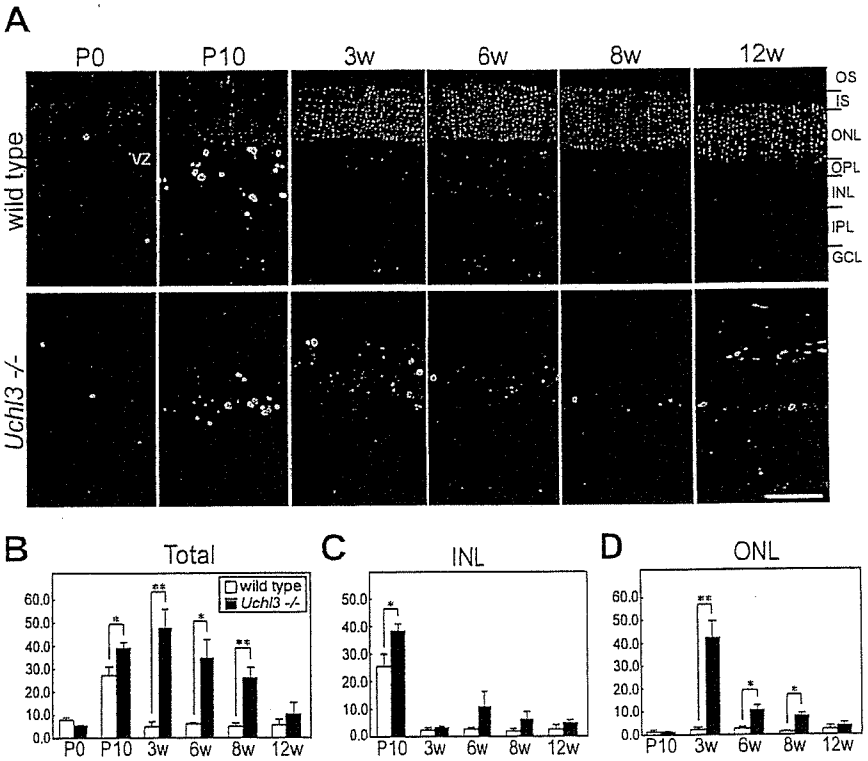

Figure 5. TUNEL analysis in wild-type and *Uchl3*-deficient mice at different ages. **A:** TUNEL staining in fluorescent microscopy shows that TUNEL-positive cells (**green**) are observed at the ventricular zone at P0 as well as at the inner nuclear layer at P10 in both genotypes. After 3w of age, TUNEL-positive cells are found in the outer nuclear layer in *Uchl3*-deficient mice. All sections are counterstained with propidium iodide (**red**). **B–D:** Number of TUNEL-positive cells in mutant mice (*Uchl3*$^{-/-}$; **black bar**) is significantly increased compared with those in wild-type (wild-type; **white bar**) at P10, 3w, 6w, and 8w (**B**). Increased number of TUNEL-positive cells in mutant mice at P10 correspond to apoptosis in the inner nuclear layer (**C**), whereas that in 3w, 6w, and 8w is reflected to apoptosis in the outer nuclear layer (**D**). VZ, ventricular zone; OS, outer segment; IS, inner segment; ONL, outer nuclear layer; OPL, outer plexiform layer; INL, inner nuclear layer; IPL, inner plexiform layer; GCL, ganglion cell layer. Scale bar = 20 μm (**A**). Each value in **B–D** represents the mean ± SE (*$P < 0.05$; **$P < 0.01$).

cient mice may be due to caspase-independent apoptotic pathway (Figure 7). Ubiquitin and Nedd-8, which are considered to be associated with UCH-L3 *in vitro*,[14,15] were expressed in the inner retina of both genotypes in a similar pattern as UCH-L1 (data not shown).

Discussion

This study demonstrates the unique localization of UCH-L3 to the photoreceptor inner segment that is abundantly populated with mitochondria after 3w of age in wild-type mice. The following features were found with regard to retinal degeneration in *Uchl3*-deficient mice. The retina showed no obvious morphological abnormalities during early postnatal development; however, progressive retinal degeneration was observed after 3w of age. The inner segment was originally perturbated with ultrastructural changes of mitochondria and increased expressions of markers for oxidative stress. The caspase-independent pathway was implicated during photoreceptor cell apoptosis. Thus, UCH-L3 may have a role in preventing mitochondrial oxidative stress-related apoptosis in photoreceptor cells.

Differential Localization of UCH-L1 and UCH-L3 in Murine Retina

The cellular distribution of UCH-L3 has not been studied except in the testis and epididymis, where UCH-L1 and UCH-L3 have distinct expression patterns.[25] In the present study, we found that UCH-L3 was enriched in the photoreceptor inner segment after 3w of age, whereas UCH-L1 was widely expressed in the inner retina. Photoreceptor cells are highly differentiated, and each segment has specific morphology and function; eg, inner segment contains abundant mitochondria,[27] and its oxygen consumption is considered to be high.[28] Meanwhile, expression of UCH-L1 at the inner retina was associated with that of ubiquitin and Nedd-8. Although *in vitro* studies indicate that UCH-L3 has de-neddylation activity,[14] UCH-L1 may be responsible for regulating expression level of ubiquitin and ubiquitin-like protein Nedd-8 in the retina. Because UCH-L1 expression in the retina was not altered in *Uchl3*-deficient mice, the function of UCH-L3 may not be compensated by UCH-L1. Our results indicate that UCH-L3 and UCH-L1 differ with regard to their localization and function in retina.

Mechanism of Photoreceptor Cell Death in the Uchl3-Deficient Mice

In our result, retinal apoptosis in *Uchl3*-deficient mice consisted of two different phases, during retinal development and after development. During the early postnatal development at P10, TUNEL-positive cells were observed in the inner nuclear layer of both genotypes, and the physiological apoptosis was slightly enhanced in the mutant retina. Because UCH-L3 was faintly expressed in the outer plexiform layer at P10 in wild-type mice, UCH-L3 may function during development. In the retinal development, the number of bipolar and Müller cell deaths reaches a peak at the postnatal days 8 to 11, which is associated with differentiation of the retina in

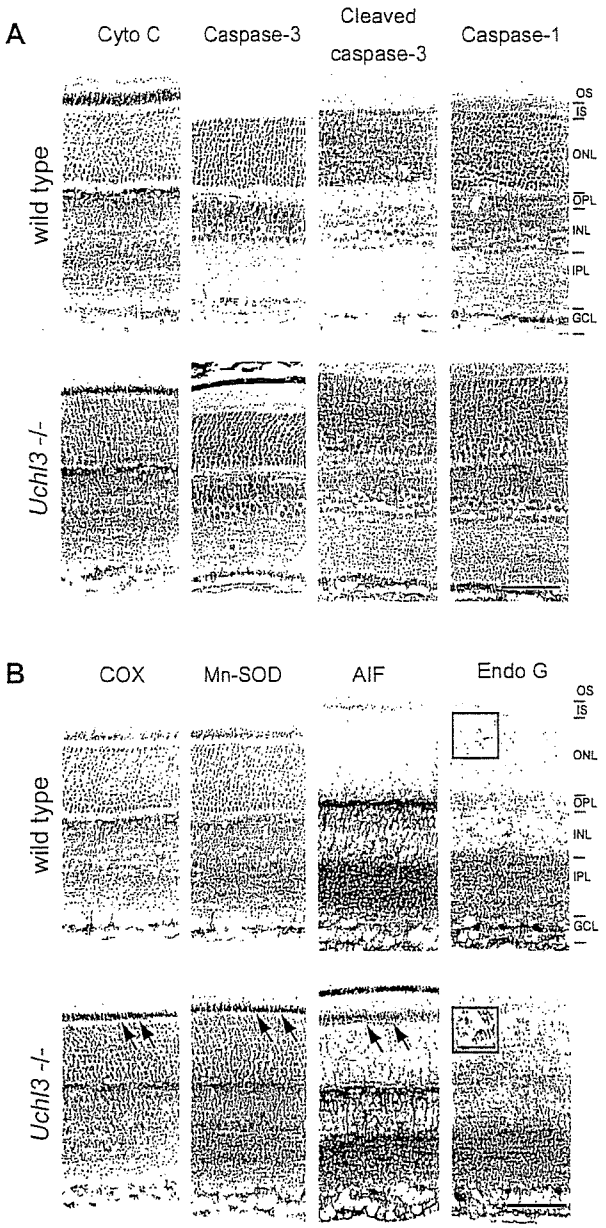

Figure 6. Immunohistochemical analysis of apoptosis- and oxidative stress-related molecules at 3w of age in wild-type and *Uchl3*-deficient mice. **A:** Expression of molecules relevant to the caspase-dependent pathway, including cytochrome *c* (Cyto C), caspase-3, cleaved caspase-3, and caspase-1, is unchanged between both genotypes. **B:** Increased immunoreactivities for oxidative stress markers, COX, Mn-SOD, and AIF, are observed in the inner segment of *Uchl3*-deficient mice (**arrows**). Translocation of Endo G to nuclei is found in the outer nuclear layer of *Uchl3*-deficient mice (**inset** in **B**). OS, outer segment; IS, inner segment; ONL, outer nuclear layer; OPL, outer plexiform layer; INL, inner nuclear layer; IPL, inner plexiform layer; GCL, ganglion cell layer. Scale bars = 50 μm (**A** and **B**); 10 μm (**inset** in **B**).

mice.[29] Therefore, loss of UCH-L3 may mildly promote the cell death of these cells.

After 3w of age, prominent and progressive photoreceptor cell apoptosis was disclosed in the outer nuclear layer of *Uchl3*-deficient mice. Under pathological conditions, several apoptotic pathways have been suggested in experimental retinal degeneration. Caspase-1 is predominantly associated with photoreceptor cell apoptosis in retinal degeneration of ischemia-reperfusion.[30] Light-induced retinal degeneration activates the parallel cascades, caspase-1[20] and caspase-independent apoptosis.[21] Oxidative stress leads to caspase-independent apoptosis in cultured cells.[31] Our results indicated that a caspase-independent pathway was activated during photoreceptor cell apoptosis in *Uchl3*-deficient mice, because immunohistochemical analysis revealed that activated caspase-3 and caspase-1 were not expressed in the degenerated retina. In addition, Endo G, a protein involved in the caspase-independent pathway, was expressed in the nuclei of the outer nuclear layer in *Uchl3*-deficient mice. Endo G is a mitochondria-specific nuclease that translocates to nuclei and serves as the DNase during a caspase-independent apoptosis.[32] Therefore, Endo G may be responsible for the DNA degradation that occurs during apoptosis in *Uchl3*-deficient mice. Expression of Endo G was slightly increased in the outer plexiform layer, inner nuclear layer, and inner plexiform layer of the *Uchl3*-deficient mice after 3w of age despite no significant UCH-L3 immunoreactivities in these layers. This result may reflect trans-synaptic secondary neuronal degeneration or glial changes of Müller cells.

AIF, another factor involved in caspase-independent apoptosis, was enriched in the inner segment; however, we did not observe translocation to nuclei for this protein. AIF is a mitochondrial flavoprotein that is a free radical scavenger of healthy cells.[33] During apoptotic induction, AIF translocates from mitochondria to nuclei.[33,34] It functions as a caspase-independent and PARP-1-dependent death effector that induces chromatin condensation and large-scale DNA fragmentation.[35] In our study, expression of AIF at the inner segment was associated with increased immunoreactivities of the oxidative stress markers, COX and Mn-SOD. Although it is unknown why AIF did not translocate to nuclei in the degenerated retina, increased immunoreactivity for AIF in the inner segment may indicate a reaction to oxidative stress. Because mouse eyes open 12 to 13 days after birth, light-induced oxidative stress may affect photoreceptor cell apoptosis in *Uchl3*-deficient mice after development. On the other hand, the retinal oxygen consumption increases under dark-adapted condition in the cat retina.[28,36] It may be interesting to study whether constant light or constant dark has any effect on the development of retinal degeneration in the *Uchl3*-deficient mice.

Uchl3-Deficient Mice as a Model of Retinal Degeneration with Mitochondrial Impairment

Apoptosis during retinal degeneration is observed in inherited diseases such as retinitis pigmentosa as well as in retinal diseases induced by a variety of stimuli, including hypoxia and oxidative stresses.[37,38] Several genetically engineered animal models of retinitis pigmentosa have been extensively investigated, including the RCS rat and *rd* mice. Retinal degeneration in the RCS rat was originally identified as an impairment of phagocytosis by pigmented epithelium due to mutation of receptor ty-

Table 1. Chronological Changes in Expression of Markers for Oxidative Stress and Caspase-Independent Apoptosis

	COX						Mn-SOD						AIF						Endo G					
	P0	P10	3w	6w	8w	12w	P0	P10	3w	6w	8w	12w	P0	P10	3w	6w	8w	12w	P0	P10	3w	6w	8w	12w
VZ*	−						−						−						−					
PR		−						−						−						−				
OS			−	−	nd	nd			−	−	nd	nd			−	−	nd	nd			−	−	nd	nd
IS			+	+	−	nd			+	+	+	nd			++	+	−	nd			−	−	−	nd
ONL		−	−	−	−	−		−	−	−	−	−		−	−	−	−	−		−	++§	+§	−	−
OPL		−	−	−	−	−		−	−	−	−	−		−	−	−	−	−		−	±	±	±	±
INL		−	−	−	−	−		−	−	−	−	−		−	−	−	−	−		−	±§	±§	−	−
IPL	−	−	−	−	−	−	−	−	−	−	−	−	−	−	−	−	−	−	−	−	−	−	±	±
GCL	−	−	−	−	−	−	−	−	−	−	−	−	−	−	−	−	−	−	−	−	−	−	−	−

*VZ, ventricular zone; PR, photoreceptor; OS, outer segment; IS, inner segment; ONL, outer nuclear layer; OPL, outer plexiform layer; INL, inner nuclear layer; IPL, inner plexiform layer; GCL, ganglion cell layer.
−, no change; ±, slight increase; +, mild increase; and ++, marked increase of immunoreactivity compared to that of wild type.
nd, not determined due to atrophic change.
§Nuclear staining.

rosine kinase (Mertk) with subsequent photoreceptor cell death occurring in a caspase-1- and -2-dependent manner.[39–42] *rd* mice have a recessive mutation in the rod cGMP phosphodiesterase β-subunit, and photoreceptor apoptosis occurs via a caspase-dependent mechanism.[43,44] Thus, these animal models of retinitis pigmentosa differ from *Uchl3*-deficient mice with regard to the mechanism of retinal degeneration.

The relationship between retinal degeneration and mitochondrial dysfunction has not been well studied except in Harlequin mice, which contain a mutation of AIF and exhibit progressive retinal degeneration.[45] We consider that the degeneration induced in the *Uchl3*-deficient mice is associated with mitochondrial dysfunction, because mitochondria in the inner segment of mutant retina exhibited morphological changes such as decreased cristae area. *Uchl3*-deficient mice reveal not only retinal degeneration but also muscle degeneration and mild growth retardation,[17] and thus the lack of UCH-L3 may affect general organs containing abundant mitochondria. Subtypes of mitochondrial diseases, such as chronic progressive external ophthalmoplegia and Kearns-Sayre syndrome, are caused by various mitochondrial DNA deletions and observed progressive ophthalmoplegia as well as retinitis pigmentosa.[46,47] Because UCH-L3 is predicted to be involved in the maintenance of mitochondrial function, *Uchl3*-deficient mice may be a model of disease that arises from mitochondrial impairment. Further studies are necessary to clarify the molecular mechanisms underlying retinal degeneration, as well as other organs in these animals.

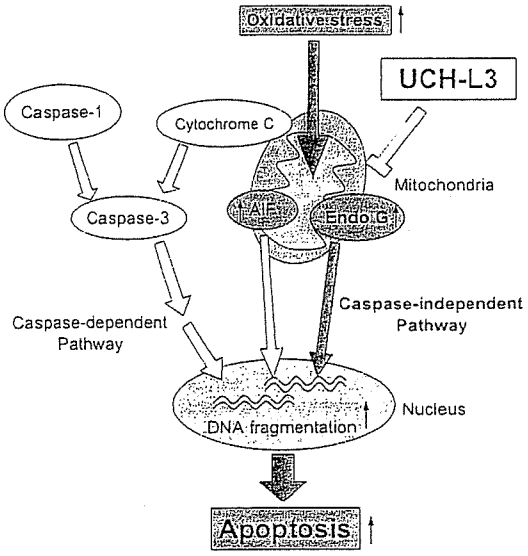

Figure 7. Function of UCH-L3 in apoptosis during retinal degeneration. Mitochondrial apoptosis is classified into caspase-dependent and caspase-independent pathways. Loss of UCH-L3 leads to oxidative stress-induced mitochondrial damage that causes translocation of Endo G from mitochondria to nuclei, resulting in caspase-independent apoptosis. **Red arrows** are considered to be activated in *Ucbl3*-deficient mice.

Acknowledgments

We thank Dr. S.M. Tilghman for providing *Uchl3*-deficient mice, Dr. K. Oyanagi, Dr. T. Harada, and Dr. K. Arima for their useful discussions, Ms. H. Fujita and Mr. D. Yamada for the breeding and care of the mice, and Mr. R. Debold, Ms. T. Matsuzawa, and Mr. N. Takagaki for editing the manuscript.

References

1. Amerik AY, Hochstrasser M: Mechanism and function of deubiquitinating enzymes. Biochim Biophys Acta 2004, 1695:189–207
2. Weissman AM: Themes and variations on ubiquitylation. Nat Rev Mol Cell Biol 2001, 2:169–178
3. Pickart CM, Eddins MJ: Ubiquitin: structures, functions, mechanisms. Biochim Biophys Acta 2004, 1695:55–72
4. Aguilar RC, Wendland B: Ubiquitin: not just for proteasomes anymore. Curr Opin Cell Biol 2003, 15:184–190
5. Wilkinson KD: Regulation of ubiquitin-dependent processes by deubiquitinating enzymes. FASEB J 1997, 11:1245–1256
6. Doran JF, Jackson P, Kynoch PA, Thompson RJ: Isolation of PGP 9.5, a new human neurone-specific protein detected by high-resolution two-dimensional electrophoresis. J Neurochem 1983, 40:1542–1547
7. Wilkinson KD, Lee KM, Deshpande S, Duerksen-Hughes P, Boss JM, Pohl J: The neuron-specific protein PGP 9.5 is a ubiquitin carboxyl-terminal hydrolase. Science 1989, 246:670–673
8. Osawa Y, Wang YL, Osaka H, Aoki S, Wada K: Cloning, expression, and mapping of a mouse gene, Uchl4, highly homologous to human and mouse Uchl3. Biochem Biophys Res Commun 2001, 283:627–633

9. Liu Y, Fallon L, Lashuel HA, Liu Z, Lansbury PT Jr,: The UCH-L1 gene encodes two opposing enzymatic activities that affect alpha-synuclein degradation and Parkinson's disease susceptibility. Cell 2002, 111:209–218
10. Leroy E, Boyer R, Auburger G, Leube B, Ulm G, Mezey E, Harta G, Brownstein MJ, Jonnalagada S, Chernova T, Dehejia A, Lavedan C, Gasser T, Steinbach PJ, Wilkinson KD, Polymeropoulos MH: The ubiquitin pathway in Parkinson's disease. Nature 1998, 395:451–452
11. Saigoh K, Wang YL, Suh JG, Yamanishi T, Sakai Y, Kiyosawa H, Harada T, Ichihara N, Wakana S, Kikuchi T, Wada K: Intragenic deletion in the gene encoding ubiquitin carboxy-terminal hydrolase in *gad* mice. Nat Genet 1999, 23:47–51
12. Wilkinson KD, Deshpande S, Larsen CN: Comparisons of neuronal (PGP 9.5) and non-neuronal ubiquitin C-terminal hydrolases. Biochem Soc Trans 1992, 20:631–637
13. Kurihara LJ, Semenova E, Levorse JM, Tilghman SM: Expression and functional analysis of *Uch-L3* during mouse development. Mol Cell Biol 2000, 20:2498–2504
14. Wada H, Kito K, Caskey LS, Yeh ET, Kamitani T: Cleavage of the C-terminus of NEDD8 by UCH-L3. Biochem Biophys Res Commun 1998, 251:688–692
15. Gan-Erdene T, Nagamalleswari K, Yin L, Wu K, Pan ZQ, Wilkinson KD: Identification and characterization of DEN1, a deneddylase of the ULP family. J Biol Chem 2003, 278:28892–28900
16. Kwon J, Wang YL, Setsuie R, Sekiguchi S, Sato Y, Sakurai M, Noda M, Aoki S, Yoshikawa Y, Wada K: Two closely related ubiquitin C-terminal hydrolase isozymes function as reciprocal modulators of germ cell apoptosis in cryptorchid testis. Am J Pathol 2004, 165:1367–1374
17. Semenova E, Wang X, Jablonski MM, Levorse J, Tilghman SM: An engineered 800 kilobase deletion of *Uchl3* and *Lmo7* on mouse chromosome 14 causes defects in viability, postnatal growth and degeneration of muscle and retina. Hum Mol Genet 2003, 12:1301–1312
18. Chang GQ, Hao Y, Wong F: Apoptosis: final common pathway of photoreceptor death in rd, rds, and rhodopsin mutant mice. Neuron 1993, 11:595–605
19. Cook B, Lewis GP, Fisher SK, Adler R: Apoptotic photoreceptor degeneration in experimental retinal detachment. Invest Ophthalmol Vis Sci 1995, 36:990–996
20. Grimm C, Wenzel A, Hafezi F, Remè CE: Gene expression in the mouse retina: the effect of damaging light. Mol Vis 2000, 6:252–260
21. Donovan M, Cotter TG: Caspase-independent photoreceptor apoptosis in vivo and differential expression of apoptotic protease activating factor-1 and caspase-3 during retinal development. Cell Death Differ 2002, 9:1220–1231
22. Osborne NN, Melena J, Chidlow G, Wood JP: A hypothesis to explain ganglion cell death caused by vascular insults at the optic nerve head: possible implication for the treatment of glaucoma. Br J Ophthalmol 2001, 85:1252–1259
23. Adler R, Curcio C, Hicks D, Price D, Wong F: Cell death in age-related macular degeneration. Mol Vis 1999, 5:31
24. Harada T, Harada C, Wang YL, Osaka H, Amanai K, Tanaka K, Takizawa S, Setsuie R, Sakurai M, Sato Y, Noda M, Wada K: Role of ubiquitin carboxy terminal hydrolase-L1 in neural cell apoptosis induced by ischemic retinal injury in vivo. Am J Pathol 2004, 164:59–64
25. Kwon J, Wang YL, Setsuie R, Sekiguchi S, Sakurai M, Sato Y, Lee WW, Ishii Y, Kyuwa S, Noda M, Wada K, Yoshikawa Y: Developmental regulation of ubiquitin C-terminal hydrolase isozyme expression during spermatogenesis in mice. Biol Reprod 2004, 71:515–521
26. Osaka H, Wang YL, Takada K, Takizawa S, Setsuie R, Li H, Sato Y, Nishikawa K, Sun YJ, Sakurai M, Harada T, Hara Y, Kimura I, Chiba S, Namikawa K, Kiyama H, Noda M, Aoki S, Wada K: Ubiquitin carboxy-terminal hydrolase L1 binds to and stabilizes monoubiquitin in neuron. Hum Mol Genet 2003, 12:1945–1958
27. De Robertis E: Electron microscope observations on the submicroscopic organization of the retinal rods. J Biophys Biochem Cytol 1956, 2:319–330
28. Linsenmeier RA, Braun RD: Oxygen distribution and consumption in the cat retina during normoxia and hypoxemia. J Gen Physiol 1992, 99:177–197
29. Young RW: Cell death during differentiation of the retina in the mouse. J Comp Neurol 1984, 229:362–373
30. Katai N, Yoshimura N: Apoptotic retinal neuronal death by ischemia-reperfusion is executed by two distinct caspase family proteases. Invest Ophthalmol Vis Sci 1999, 40:2697–2705
31. Carmody RJ, Cotter TG: Oxidative stress induces caspase-independent retinal apoptosis in vitro. Cell Death Differ 2000, 7:282–291
32. Li LY, Luo X, Wang X: Endonuclease G is an apoptotic DNase when released from mitochondria. Nature 2001, 412:95–99
33. Susin SA, Lorenzo HK, Zamzami N, Marzo I, Snow BE, Brothers GM, Mangion J, Jacotot E, Costantini P, Loeffler M, Larochette N, Goodlett DR, Aebersold R, Siderovski DP, Penninger JM, Kroemer G: Molecular characterization of mitochondrial apoptosis-inducing factor. Nature 1999, 397:441–446
34. Lorenzo HK, Susin SA, Penninger J, Kroemer G: Apoptosis inducing factor (AIF): a phylogenetically old, caspase-independent effector of cell death. Cell Death Differ 1999, 6:516–524
35. Yu SW, Wang H, Poitras MF, Coombs C, Bowers WJ, Federoff HJ, Poirier GG, Dawson TM, Dawson VL: Mediation of poly(ADP-ribose) polymerase-1-dependent cell death by apoptosis-inducing factor. Science 2002, 297:259–263
36. Linsenmeier RA: Effects of light and darkness on oxygen distribution and consumption in the cat retina. J Gen Physiol 1986, 88:521–542
37. Pacione LR, Szego MJ, Ikeda S, Nishina PM, McInnes RR: Progress toward understanding the genetic and biochemical mechanisms of inherited photoreceptor degenerations. Annu Rev Neurosci 2003, 26:657–700
38. Phelan JK, Bok D: A brief review of retinitis pigmentosa and the identified retinitis pigmentosa genes. Mol Vis 2000, 6:116–124
39. D'Cruz PM, Yasumura D, Weir J, Matthes MT, Abderrahim H, LaVail MM, Vollrath D: Mutation of the receptor tyrosine kinase gene Mertk in the retinal dystrophic RCS rat. Hum Mol Genet 2000, 9:645–651
40. Feng W, Yasumura D, Matthes MT, LaVail MM, Vollrath D: Mertk triggers uptake of photoreceptor outer segments during phagocytosis by cultured retinal pigment epithelial cells. J Biol Chem 2002, 277:17016–17022
41. Katai N, Kikuchi T, Shibuki H, Kuroiwa S, Arai J, Kurokawa T, Yoshimura N: Caspase-like proteases activated in apoptotic photoreceptors of Royal College of Surgeons rats. Invest Ophthalmol Vis Sci 1999, 40:1802–1807
42. Vollrath D, Feng W, Duncan JL, Yasumura D, D'Cruz PM, Chappelow A, Matthes MT, Kay MA, LaVail MM: Correction of the retinal dystrophy phenotype of the RCS rat by viral gene transfer of Mertk. Proc Natl Acad Sci USA 2001, 98:12584–12589
43. Jomary C, Neal MJ, Jones SE: Characterization of cell death pathways in murine retinal neurodegeneration implicates cytochrome c release, caspase activation, and bid cleavage. Mol Cell Neurosci 2001, 18:335–346
44. Lem J, Flannery JG, Li T, Applebury ML, Farber DB, Simon MI: Retinal degeneration is rescued in transgenic rd mice by expression of the cGMP phosphodiesterase β subunit. Proc Natl Acad Sci USA 1992, 89:4422–4426
45. Klein JA, Longo-Guess CM, Rossmann MP, Seburn KL, Hurd RE, Frankel WN, Bronson RT, Ackerman SL: The harlequin mouse mutation downregulates apoptosis-inducing factor. Nature 2002, 419:367–374
46. Land JM, Morgan-Hughes JA, Hargreaves I, Heales SJ: Mitochondrial disease: a historical, biochemical, and London perspective. Neurochem Res 2004, 29:483–491
47. Schmiedel J, Jackson S, Schäfer J, Reichmann H: Mitochondrial cytopathies. J Neurol 2003, 250:267–277

WILEY InterScience® DISCOVER SOMETHING GREAT

JOURNAL OF CELLULAR PHYSIOLOGY 209:172–182 (2006)

Parkin Potentiates ATP-Induced Currents Due to Activation of P2X Receptors in PC12 Cells

AYUMI SATO,[1] YUKIKO ARIMURA,[1] YOSHIMASA MANAGO,[1] KAORI NISHIKAWA,[2] KUMIKO AOKI,[2] ETSUKO WADA,[2] YASUYUKI SUZUKI,[2] HITOSHI OSAKA,[2,3] RIEKO SETSUIE,[1,2] MIKAKO SAKURAI,[1,2] TAIJU AMANO,[1,2] SHUNSUKE AOKI,[2,4] KEIJI WADA,[2] AND MAMI NODA[1]*

[1]*Laboratory of Pathophysiology, Graduate School of Pharmaceutical Sciences, Kyushu University, Fukuoka, Japan*

[2]*Department of Degenerative Neurological Diseases, National Institute of Neuroscience, National Center of Neurology and Psychiatry, Tokyo, Japan*

[3]*Information and Cellular Function, PRESTO, Japan Science and Technology Corporation (JST), Kawaguchi, Saitama, Japan*

[4]*NEDO (New Energy and Industrial Technology Development Organization), Kawasaki, Kanagawa, Japan*

Loss-of-function mutations of the parkin gene causes an autosomal recessive juvenile-onset form of Parkinson's disease (AR-JP). Parkin was shown to function as a RING-type E3 ubiquitin protein ligase. However, the function of parkin in neuronal cells remains elusive. Here, we show that expression of parkin-potentiated adenosine triphosphate (ATP)-induced currents that result from activation of the P2X receptors which are widely distributed in the brain and involved in neurotransmission. ATP-induced inward currents were measured in mock-, wild-type or mutant (T415N)-parkin-transfected PC12 cells under the conventional whole-cell patch clamp configuration. The amplitude of ATP-induced currents was significantly greater in wild-type parkin-transfected cells. However, the immunocytochemical study showed no apparent increase in the number of P2X receptors or in ubiquitin levels. The increased currents were attenuated by inhibition of cAMP-dependent protein kinase (PKA) but not protein kinase C (PKC) or Ca^{2+} and calmodulin-dependent protein kinase (CaMKII). ATP-induced currents were also regulated by phosphatases and cyclin-dependent protein kinase 5 (CDK5) via dopamine and cyclic AMP-regulated phosphoprotein (DARPP-32), though the phosphorylation at Thr-34 and Thr-75 were unchanged or rather attenuated. We also tried to investigate the effect of α-synuclein, a substrate of parkin and also forming Lysine 63-linked multiubiquitin chains. Expression of α-synuclein did not affect the amplitude of ATP-induced currents. Our finding provides the evidence for a relationship between parkin and a neurotransmitter receptor, suggesting that parkin may play an important role in synaptic activity. J. Cell. Physiol. 209: 172–182, 2006. © 2006 Wiley-Liss, Inc.

Recessive juvenile-onset form of Parkinson's disease (AR-JP) is the most frequent form of familial Parkinson's disease (PD). Mutations in the parkin gene were originally discovered from the linkage study of Japanese AR-JP families (Kitada et al., 1998). Thereafter its mutations have been found worldwide and parkin gene is now accepted as one of eight genes responsible for Parkinson's disease (see review by Cookson, 2005).

It has been demonstrated that parkin is associated with the ubiquitin–proteasome system. Wild-type parkin encodes for a protein-ubiquitin E3 ligase, which ubiqutinates many substrate proteins to enhance their degradation by the 26S proteasomes (Imai et al., 2000; Shimura et al., 2000; Zhang et al., 2000). As parkin mutations lose their E3 ligase activity, it is thought that accumulation of parkin substrate may lead to the selective death of catecholaminergic cell death (Ko et al., 2005) and familial-associated mutations differentially disrupt the solubility, localization, binding, and unibiquitination properties of parkin (Sriram et al., 2005).

It is reported that parkin is localized on surface of synaptic vesicle membranes (Kubo et al., 2001). As substrates of parkin, some synaptic proteins were reported, such as synaptotagmin XI (Huynh et al., 2003), septin CDCrel-1 (Zhang et al., 2000), and synphylin1 (Lim et al., 2005), suggesting that parkin may have a neuronal function. However, the nature of this function is unknown. Therefore, we have investigated the effect of parkin on one of receptor channels that affect neurotransmitter secretion.

Adenosine triphosphate (ATP) and related nucleotides induce a release of catecholamines, including dopamine, in PC12 pheochromocytoma cells, a frequently used model for sympathetic neurons (Sela et al., 1991; Nakazawa and Inoue, 1992). ATP receptors are divided into two subtypes, P2X and P2Y receptors.

Ayumi Sato and Yukiko Arimura contributed equally to this work.

Contract grant sponsor: Japan Society for Promotion of Science; Contract grant number: 15082214; Contract grant sponsor: Ministry of Education, Culture, Sports, Science and Technology, Japan; Contract grant number: 16300126; Contract grant sponsor: Ministry of Health, Labour and Welfare, Japan; Contract grant sponsor: National Institute of Biomedical Innovation (NIBIO) Japan; Contract grant number: 05-32.

Yoshimasa Manago's present address is Foods and Fine Chemicals Department, Products Development Section, Maruha Corporation, Tochigi 321-3231, Japan.

Hitoshi Osaka's present address is Division of Neurology, Clinical Research Institute, Kanagawa, Children's Medical Center, Yokohama, 232-8555, Japan.

*Correspondence to: Mami Noda, Laboratory of Pathophysiology, Graduate School of Pharmaceutical Sciences, Kyushu University, 3-1-1 Maidashi, Higashi-ku, Fukuoka 812-8582, Japan.
E-mail: noda@phar.kyushu-u.ac.jp

Received 8 October 2005; Accepted 5 June 2006

Published online in Wiley InterScience (www.interscience.wiley.com.), 6 July 2006.
DOI: 10.1002/jcp.20719

P2X receptors are ionotropic receptors and form cationic channels, while P2Y receptors are G-protein-coupled receptors. Recently, we have reported that P2X receptor-induced membrane currents were augmented by ubiquitin carboxy-terminal hydrolase L1 (UCH-L1), presumably due to upregulation of mono-ubiquitin level (Manago et al., 2005). Therefore, the ubiquitin–proteasome pathway is also implicated in the function of ATP receptors.

In the present study, we analyzed relationships between parkin and P2X receptors by expressing parkin or a familial-linked mutant parkin (T415N-parkin) which lacks ubiquitin E3 ligase activity in PC12 cells. This is the first evidence to show the relationship between physiological function of parkin and receptor channels involved in neurotransmitter secretion. These findings may help to understand the function of parkin in the nervous system and the mechanism of Parkinson's disease caused by dysfunction of parkin.

MATERIALS AND METHODS

Chemicals

RPMI-1640 medium, ATP-2Na, H-89 (N-[2-(p-bromoocinamylamino)ethyl]-5-isoquinolinesulfonamide), H-85, chelerythrine, roscovitine (2-(R)-(1-Ethyl-2-hydroxyethylamino)-6-benzylamino-9-isopropylpurine), and PD98059 (2′-Amino-3′-methoxyflavone) were from Sigma (St. Louis, MO). Nerve growth factor (NGF) and Lipofectamine 2000 were from Invitrogen (Carlsbad, CA). KN-93 (2-[N-(2-hydroxyethyl)]-N-(4-methoxybenzenesulfonyl))amino-N-(4-chlorocinnamyl)-N-methylbenzylamine) and okadaic acid was from Calbiochem (San Diego, CA).

Cell culture

PC12 Tet-off cells were grown in RPMI-1640 medium containing 5% fetal bovine serum (FBS) (Cell Culture Technologies, Lugano, Switzerland), 10% horse serum (HS) (Invitrogen), 100 units/ml penicillin (Life Technologies, Rockville, MD), and 100 μg/ml streptomycin (Life Technologies) in a humidified atmosphere with 10% CO_2 at 37°C. To differentiate cells, 100 ng/ml of NGF was added to the RPM 1640 medium with 0.1% HS, 0.05% FBS, 50 unit/ml penicillin, and 100 μg/ml streptomycin for 4 days.

Transfection

Plasmids used for transfection were constructed using pIRES-EYFP vector (Clontech, Nottinghamshire, UK). For electrophysiological recording, PC12 Tet-Off cells were transfected with mock, Flag-tagged wild-type or mutant (T415N) parkin cDNA, using Lipofectamine 2000. The engineered PC12 cells are constructed to have higher transfection efficiency than wild-type PC12 cells (unpublished data). After 24 h of transfection, cells were treated with NGF and differentiated for 4–5 days. More precisely, 3.0×10^5 cells were seeded in 35-mm dishes in RPMI with 10% HS and 5% FBS. Twenty-four hours after seeding, the medium was replaced with 500 μl of serum-free RPMI 1640 medium. Then, the transfection mixture containing 4 μg of cDNA and 10 μl of Lipofectamine 2000 in 500 μl of RPMI-1640 was added to each dish and incubated for 6 h in a humidified atmosphere with 10% CO_2 at 37°C. One milliliter of complete RPMI-1640 supplemented with an additional 10% HS and 5% FBS was then added to each dish. The solution for transfection was discarded 18 h later and replaced with RPMI-1640 medium for differentiation with added 100 ng/ml NGF. For transfection of α-synuclein, plasmids were constructed using pIRES-EGFP vector (Clontech) and the same protocol was used as for parkin. For protein analysis, cells (7.5×10^5/well, Clontech) were transfected in the same way. After 24 h, cells were subjected to Western blot analysis.

Western blot analysis

After 48 h of transfection of pIRES-EYFP-mock, pIRES-EYFP-Flag-wild-type parkin, or -T415N parkin with Lipofectamine 2000 (Invitrogen), cells were lysed with TBS buffer (25 mM Tris/150 mM NaCl, PH 7.4) containing 1% Triton X-100 and centrifuged at 15,000 rpm for 30 min at 4°C. Thirty micrograms of each protein was subjected to SDS–PAGE on a 15% gel and transferred to PVDF membranes (Bio Rad, CA) and immunoblotted with anti-Flag M2 (1:200, Sigma, monoclonal) or anti-Actin (1:200, Chemicon, Temecula, CA, monoclonal).

Immunocytochemical analysis

After transfection, cells were fixed with 4% paraformaldehyde. Immunocytochemistry on PC12 Tet-Off cells was performed as previously described (Osaka et al., 2003) using antibodies against parkin (5 μg/ml, Zymed, San Francisco, CA; monoclonal), $P2X_2$, $P2X_4$, or $P2X_6$ receptor (1:200, Alomone labs, Jerusalem, Israel; polyclonal), ubiquitin that is predominantly reactive to free ubiquitin in immunohistochemistry (1:100, Sigma; polyclonal), α-synuclein (1:500, BD Biosciences, San Jose, CA), and dopamine and cyclic AMP-regulated phosphoprotein (DARPP-32) (phosphor Thr-34 and phospho Thr-75) (1:500, Abcam, Cambridge, UK). For immunofluorescence studies, anti-rabbit IgG conjugated with Cy3 antibodies (1:200, Jackson Immuno Research, West Grove, PA) or Alexa Fluor 568 goat anti-mouse (1:250, Molecular Probes, Invitrogen) was used as secondary antibodies. The same strength of the laser wavelength or fluorescence was applied in the series of images, for the quantification of the fluorescence under the confocal laser microscope system (LSM510, Carl Zeiss, Oberkochen, Germany).

Electrophysiological measurements

Cells expressing EYFP were selected under the fluorescence microscope. A patch pipette was then applied to the cell to obtain a giga-ohm seal under phase-bright mode. Whole-cell membrane current recordings were made under voltage-clamp at a holding potential of −70 mV as reported previously (Noda et al., 2000; Manago et al., 2005), using an Axopatch-200B amplifier (Axon Instruments, Foster City, CA). The patch pipette was filled with a solution containing (in mM): CsCl, 120; Mg_2ATP_3, 3; HEPES, 20; $CaCl_2$, 1; $MgCl_2$, 1; EGTA, 5. The pH of the solution was adjusted to 7.2 with 1 N CsOH. The pipette resistance was 5–9 MΩ. The external solution contained (mM): NaCl, 132; KCl, 5; $CaCl_2$, 2; $MgCl_2$, 1; glucose, 10; and HEPES, 10. The pH was adjusted to 7.4 with 1 N NaOH. External ATP or drugs were applied rapidly using the 'Y tube' technique (Min et al., 1996), which allows the complete exchange of the external solution surrounding a cell within 20 msec. Temperature monitored in the recording dishes was 33–34°C.

In the experiments using inhibitors (except PD98059), ATP was applied twice to ensure reproducibility of the ATP-induced current in control experiments. The inhibitor solution was applied after first application of ATP for a period appropriate to the inhibitor until the end of second application of ATP. The current amplitude obtained at the second application of ATP with or without inhibitors was normalized to that of the first ATP-induced current. All values were presented as mean ± SEM. Statistical analysis was done using ANOVA. A value of $P < 0.05$ was considered to be the minimum level of significance. Curve fitting was performed using the standard Hill Equation (Igor Pro 4.07; Wavemetrics, Lake Oswego, OR).

RESULTS

Transfection of parkin in PC12 Tet-Off cells

Expression of plasmid constructs was first examined in PC12 Tet-Off cells. Western blot analysis showed immunoreactive bands by anti-Flag antibodies in cells transfected with pIRES-EYFP-wild type parkin or T415N parkin, but not with mock plasmids (Fig. 1A). The efficiency of the transfection was about 10% in PC12 Tet-Off cells. To test endogenous expression of parkin, cells were immunostained using specific antibodies for parkin. The strong expression of parkin (red) was observed in wild-type parkin-transfected cell (yellow) but not in non-transfected cells in the same field (shown

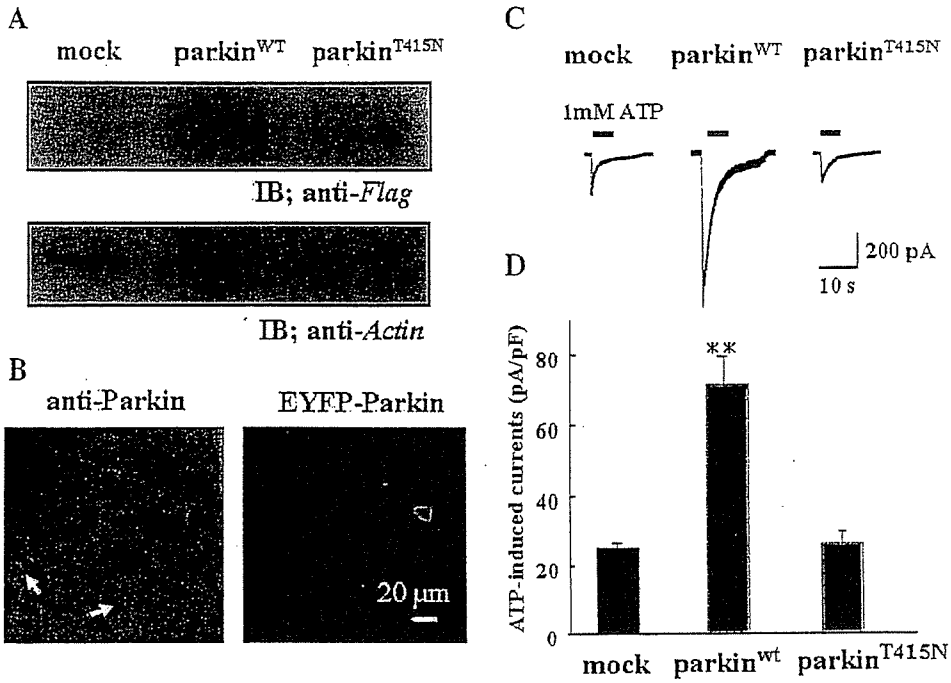

Fig. 1. Transfection of parkin and potentiation of ATP-induced currents in PC12 cells. A: Western blot analysis of PC12 Tet-Off cells. Cells were transfected with either pIRES-EYFP-mock, wild-type (WT) parkin, or T415N parkin. Each protein was subjected to SDS–PAGE and immunoblotted with anti-Flag or anti-Actin antibody. B: Confocal image of PC12 Tet-Off cells transfected with pIRES-EYFP-wild-type parkin (yellow) showed strong expression level of parkin (red) while non-transfected cells (white arrows) showed little expression of parkin. C: Inward membrane currents induced by 1 mM ATP at the holding potential of −70 mV in mock-, wild-type parkin-, and T415N parkin-transfected PC12 Tet-Off cells. D: Amplitudes of peak inward currents induced by 1 mM ATP in mock-, wild-type parkin-, and T415N parkin-transfected PC12 Tet-Off cells. The bars represent the mean ± SEM, $^{**}P < 0.01$.

with white arrows in Fig. 1B), suggesting little endogenous parkin was expressed in PC12 Tet-Off cells.

Effects of expression of parkin on ATP-induced currents

ATP-activated inward currents due to the activation of P2X receptors at negative holding potentials in PC12 cells or PC12 Tet-Off cells have been reported previously (Nakazawa et al., 1994; Manago et al., 2005). In our experiments, PC12 Tet-Off cells were voltage-clamped at −70 mV and 1 mM ATP were applied to see whether or not overexpression of parkin affected maximum inward currents. In parkin-transfected cells, ATP-induced inward currents were nearly threefold larger than those in mock- or mutant (T415N) parkin-transfected cells (Fig. 1C). The amplitudes of the peak inward currents in mock-, wild-type parkin-, and T415N parkin-transfected PC12 Tet-Off cells were 24.8 ± 1.6 pA/pF (n = 9), 71.3 ± 8.4 pA/pF (n = 5), and 26.1 ± 3.4 pA/pF (n = 7), respectively (Fig. 1D).

The current–voltage relationships of the ATP-induced inward currents were determined by applying 50 msec voltage steps in 10 mV increments between −100 mV and +50 mV at 50 msec interval from the holding potential of −70 mV before and during the application of ATP (Fig. 2A). Current traces obtained before and after application of ATP in wild-type parkin-transfected cells are shown in Figure 2B. The current levels at the end of each pulse before and during ATP application were measured in mock-, wild-type parkin-, or T415N parkin-transfected cells. The amplitudes of the ATP-induced currents at each voltage were obtained by subtracting the one before application of ATP from the one during application of ATP. The current–voltage relationships obtained at the time point after 40 msec from the beginning of each pulse were plotted as in Figure 2C. To allow for possible desensitization, the current–voltage relationships were also obtained by applying voltage steps in the opposite direction, that is, from +50 to −100 mV, but there was little change (data not shown). The reversal potential was about 0 mV, suggesting that these currents were due to non-specific cationic channels.

ATP-induced inward currents were concentration-dependent. Mock- and T415N parkin-transfected cells showed visible ATP-induced inward currents at 0.03 nM and a maximum response at 1 mM ATP (Fig. 3A). The maximum response was almost three times bigger in wild-type parkin-transfected cells (Fig. 3B). The sensitivity to ATP was not significantly changed by overexpression of either mock, wild-type, or T415N parkin. EC_{50} values (half maximum concentration) were 187 ± 45 μM, 127 ± 13 μM, and 177 ± 124 μM with Hill coefficients (n_H) of 1.05 ± 0.314, 0.97 ± 0.12, and 2.00 ± 2.26 in mock-, wild-type, and T415N parkin-transfected cells, respectively.

Expression of $P2X_2$, $P2X_4$, and $P2X_6$ receptors in parkin-transfected cells

In PC12 cells, $P2X_2$ and $P2X_4$ receptors (Hur et al., 2001) with lower level of $P2X_6$ receptor are expressed (our unpublished data). It was possible that the expression of P2X receptors was enhanced by overexpression of parkin. To define the changes in the expression level of P2X receptors semi-quantitatively, $P2X_2$, $P2X_4$, and $P2X_6$ receptors were immunostained using specific antibodies for each receptor subtype. The subcellular localization of $P2X_2$, $P2X_4$, and $P2X_6$ receptors showed no obvious difference in wild-type parkin-transfected cells compared with non-transfected cells in the same field (Fig. 4), suggesting that the potentiation of the

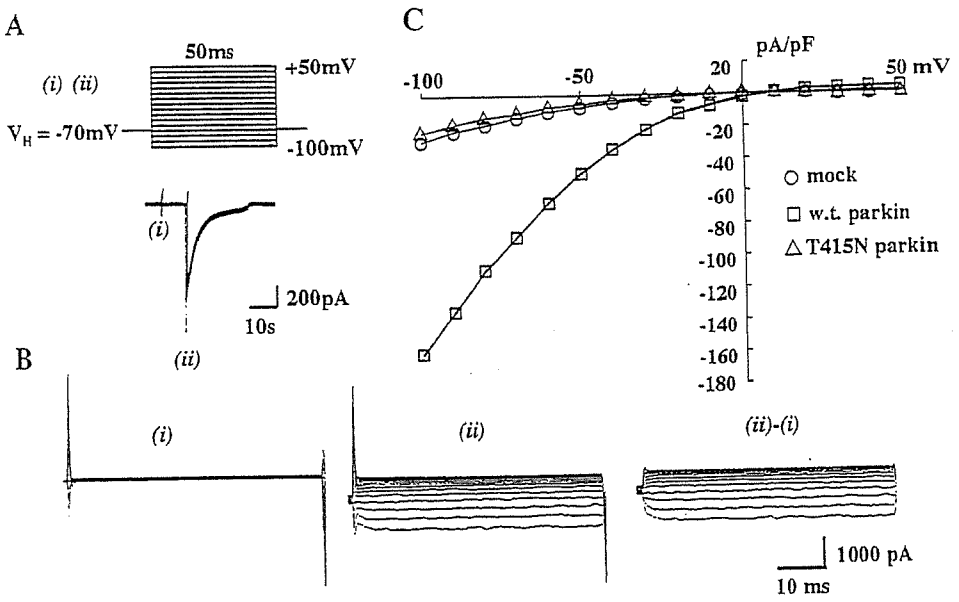

Fig. 2. Voltage-dependency of ATP-induced currents in mock-, wild-type parkin-, and T415N parkin-transfected PC12 Tet-Off cells. A: The voltage protocol shown in the upper part was applied before and during application of 1 mM ATP at the time indicated by (i) and (ii) in the lower part. B: Cumulated current traces obtained in wild-type parkin-transfected cells before (i) and during (ii) application of ATP. The subtracted currents [(ii) – (i)] show the ATP-induced currents. C: The current–voltage relationships of ATP-induced currents. The amplitudes of subtracted currents [(ii) – (i)] in (B) at the end of 50 msec pulses were plotted against the pulse potentials in mock (○)-, wild-type (w.t.) parkin (□)-, and T415N parkin (△)-transfected cells.

ATP-induced currents was not due to an increase in the total number of P2X receptors.

Expression of mono-ubiquitin in parkin-transfected cells

It has previously been reported that a de-ubiquitinating isozyme, ubiquitin carboxy-terminal hydrolase L1 (UCH-L1), also potentiated ATP-induced currents (Manago et al., 2005). However, hydrolase activity was not involved in the potentiation of ATP-induced currents because a mutant form lacking hydrolase activity also potentiated the current. Instead, UCH-L1 upregulated ubiquitin levels (Osaka et al., 2003) and overexpression of UCH-L1 in PC12 cells increased the mono-ubiquitin level (Manago et al., 2005). To test whether or not parkin also upregulate mono-ubiquitin levels, ubiquitin was stained using anti-mono-ubiquitin IgG. Unlike the effect of UCH-L1, immunoreactivity for ubiquitin in wild-type parkin-transfected cells was unchanged compared to that in mock-transfected cells or non-transfected cells in the same field (Fig. 5). These results indicated that parkin did not upregulate mono-ubiquitin.

Little effects of α-synuclein on ATP-induced currents

Since it has recently been shown that UCH-L1, parkin, and α-synuclein form lysine 63-linked multi-ubiquitin chains (Doss-Pepe et al., 2005; Lim et al.,

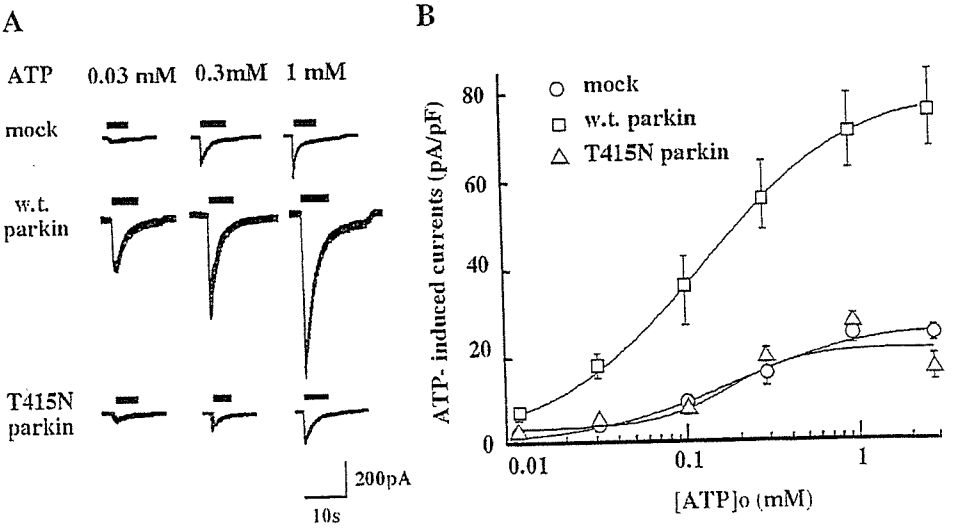

Fig. 3. Concentration-dependent curve of ATP-induced currents in mock-, wild-type parkin-, and T415N parkin-transfected PC12 Tet-Off cells. A: Inward membrane currents induced by 0.03, 0.1, and 1 mM ATP at the holding potential of −70 mV in mock-, wild-type (w.t.) parkin-, and T415N parkin-transfected PC12 Tet-Off cells. B: The peak inward current induced by ATP at the holding potential of −70 mV was plotted against the ATP concentration at several points between 0.01 and 3 mM in mock (○)-, wild-type parkin (□)-, and T415N parkin (△)-transfected PC12 Tet-Off cells. Each point represents the mean of 5–13 cells and the bar shows the mean ± SEM. The curve shows the least squares fit.

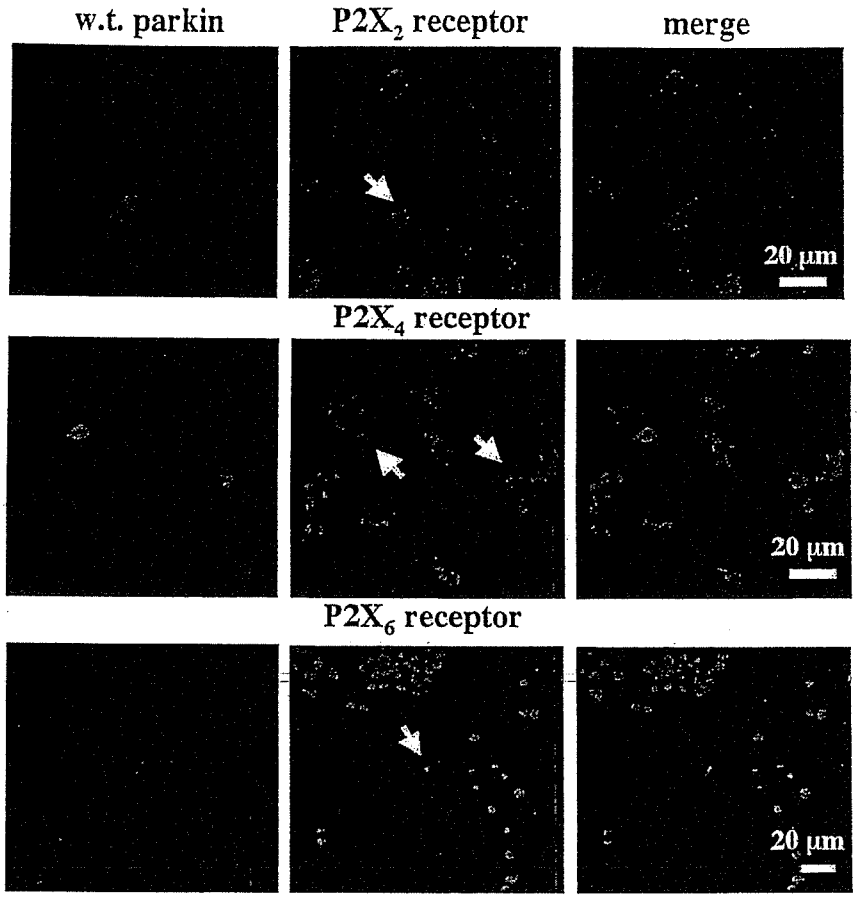

Fig. 4. Parkin has no clear effect on the expression of $P2X_2$, $P2X_4$, and $P2X_6$ receptors. Confocal images of PC12 Tet-Off cells transfected with pIRES-EYFP-wild-type (w.t.) parkin that were double stained with $P2X_2$ (**upper part**), $P2X_4$ (**middle part**), and $P2X_6$ receptors (**lower part**). EYFP (yellow)-positive cells were parkin-transfected cells, showing similar expression level of P2X receptors (red) to those in non-transfected cells.

2005), α-synuclein also might have a similar effect on P2X receptor. Transfection of α-synuclein was performed in the same way as parkin and the transfection efficiency was much greater than that of parkin (up to 30%) and the protein expression was confirmed by Western blotting (not shown). The strong expression of α-synuclein (red) was observed in transfected cell (green) but not in non-transfected cells in the same field

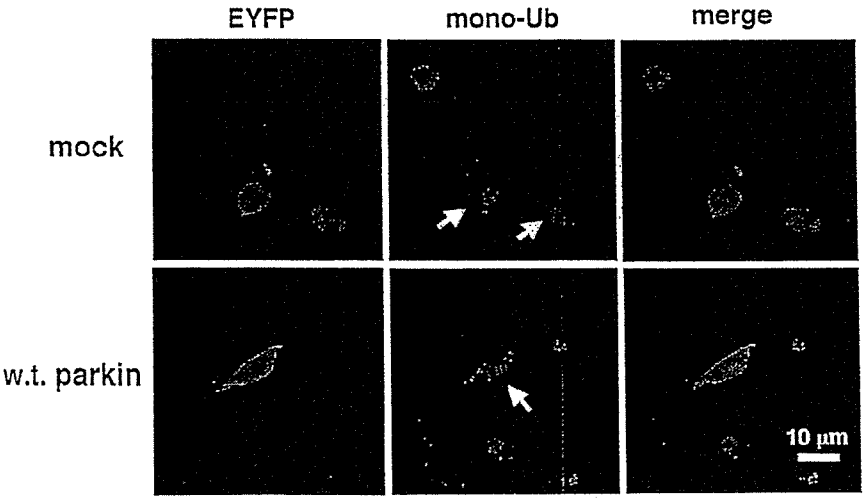

Fig. 5. Parkin had no clear effect on mono-ubiquitin expression. Confocal images of PC12 cells transfected with pIRES-mock or wild-type (w.t.) parkin that were double stained with mono-ubiquitin (red) and EYFP (yellow).